Enhanced Gas Absorption in the Ionic Liquid 1-n-Hexyl-3-methylimidazolium Bis(Trifluoromethylsulfonyl)amide ([hmim][Tf_2N]) Confined in Silica Slit Pores: A Molecular Simulation Study

Wei Shi,[*,†,‡,¶] and David R. Luebke[†]

U. S. Department of Energy, National Energy Technology Laboratory, Pittsburgh, PA 15236, USA, URS Corporation, South Park, PA 15129, USA, and Department of Chemical and Petroleum Engineering, University of Pittsburgh, Pittsburgh, PA 15261, USA

E-mail: shiw@netl.doe.gov

Abstract

Two-dimensional $NP_{xy}T$ and isostress-osmotic ($N_2P_{xy}Tf_1$) Monte Carlo simulations were used to compute the density and gas absorption properties of the ionic liquid (IL) 1-n-hexyl-3-methylimidazolium bis(Trifluoromethylsulfonyl)amide ([hmim][Tf_2N]) confined in silica slit pores (25-45 Å). Self-diffusivity values for both gas and IL were calculated from NVE molecular dynamics simulations using both smooth and atomistic potential models for the silica. Simulations show that the molar volume for [hmim][Tf_2N] confined in 25-45 Å silica slit

[*]To whom correspondence should be addressed
[†]U. S. Department of Energy, National Energy Technology Laboratory, Pittsburgh, PA 15236, USA
[‡]URS Corporation, South Park, PA 15129, USA
[¶]Department of Chemical and Petroleum Engineering, University of Pittsburgh, Pittsburgh, PA 15261, USA

pores are 12-31% larger than for the bulk IL at 313-573 K and 1 bar. The amounts of CO_2, H_2, and N_2 absorbed in the confined IL are typically 1.1-3 times larger than in the bulk IL due to larger molar volumes for the confined IL compared to the bulk IL. The CO_2, N_2, and H_2 molecules are generally absorbed close to the silica wall where the IL density is very low. This arrangement causes the self-diffusivities for these gases in the confined IL to be 2 to 8 times larger than in the bulk IL at 298-573 K. The solubility for water in the confined and bulk ILs are similar, which is likely due to strong water interactions with [hmim][Tf_2N] through hydrogen-bonding resulting in the confined IL molar volume playing a less important role in determining H_2O solubility. Water molecules were largely absorbed in the IL-rich region rather than close to the silica wall. The self-diffusivities for water correlate with the confined IL. The confined IL exhibits self-diffusivities larger than the bulk IL at lower temperatures, but smaller than the bulk IL at higher temperatures. The findings from simulations are consistent with available experimental data for similar confined IL systems.

1 Introduction

Ionic liquids (ILs) have received intense attention due to their unique properties, such as low vapor pressure, nonflammability, wide liquid temperature range, wide electrochemical window, high thermal stability, and high solvating capacity for both polar and nonpolar compounds.[1,2] Generally, ILs are very viscous with viscosity values typically 2-3 orders of magnitude larger than water. Although highly viscous ILs are favored in certain applications such as stationary phases for gas-liquid chromatography,[3] the high viscosity will cause many serious problems in chemical processing, such as requiring much more power to pump the IL and significantly slowing down mass and heat transfer for gas absorption and reaction in ILs. Consequently, new devices and/or novel methods have to be developed to improve mass and heat transfer in ILs before the ILs are adopted in large-scale industrial applications.

In order to improve mass transfer for gas absorption in ILs, molecular simulations have been conducted which show CO_2 self-diffusion coefficients increase 17 times in [hmim][Tf_2N] confined

in a (20,20) carbon nanotube (CNT) (diameter 27 Å) compared to the un-confined bulk IL. Additionally, the confined IL exhibits self-diffusivity 1-2 orders of magnitude larger than the bulk IL.[4] The enhanced self-diffusivity values for both gas and confined IL were mainly ascribed to the smoothness of the CNT and larger molar volumes for the confined IL compared to the bulk IL.[4] Recently, Hung and coworkers completed a series of theoretical studies for IL confined in nano-materials. They have found that the IL self-diffusivity under confinement is very heterogeneous due to different packing of the IL in nano-materials.[5] The confined IL could diffuse faster than the bulk IL depending on the IL loading and the pore size of the nano-material.[6] Intrigued by our theoretical work, Iocab et al. have experimentally determined that the self-diffusivity coefficients for confined [bmim][BF_4] in silica nanopores (pore size 75-104 Å) are increased by two orders of magnitude compared to the bulk IL.[7] The authors attributed the enhanced IL self-diffusivity to the changes in ion packing and the reduction of the density for IL in small pores,[7] which are also consistent with our simulations.[4] Recently, Baltus[8] and colleagues performed an experimental investigation of the CO_2 absorption behavior in confined IL. They found that CO_2 permeability in ILs supported in the alumina nanopores (200 Å and 1000 Å) could be increased four times compared to the permeability in the bulk IL.

In spite of the above progress, some important questions are yet to be addressed. For example, even though CO_2 permeabilities (solubility $\times$ diffusivity) in the alumina-pore confined ILs are larger than in the corresponding bulk ILs,[8] it is unclear how confinement affects the CO_2 solubility and diffusivity. Although the confined IL exhibits much larger self-diffusivity values than the bulk IL at low temperatures, Iacob et al. also found that at higher temperatures the silica-confined IL exhibits smaller self-diffusivity than the bulk IL.[7] These temperature-dependent confinement effects on IL self-diffusivity were not observed in our previous simulations for the CNT-confined IL.[4] The 1-dimensional (D) CNT interacts more strongly with the ILs than the 2-D graphite and silica systems. It would be interesting to investigate whether ILs confined in the weakly interacting silica pores still exhibit similar enhanced gas solubility and diffusivity behaviors compared to ILs confined in the strongly interacting CNT. Answering these questions will help researchers to

enhance IL properties in a variety of applications including reaction media, nonvolatile electrolytes, separation solvents, and gas separation. Additionally, investigation of the confinement effects in a simple silica slit pore on gas absorption would help pave the way to model IL confined in the more realistic and more complicated MCM-41 pores.

Here we addressed the above questions using molecular modeling. We have systematically studied CO_2, H_2, N_2, and H_2O gas absorption in [hmim][Tf_2N] confined in silica slit pores with widths between 25 Å and 45 Å. The pore sizes of 25-45 Å were chosen because [hmim][Tf_2N] exhibits several cation and anion layers in these pores, which allows us to study the pore size effects on IL properties for gas absorption. Additionally, simulation results in these silica pores will be compared with the previous work for the same IL confined in a (20,20) CNT with a diameter of 27 Å.[4] Finally, these silica pore sizes are similar to the pore size values for the MCM-41 (20-50 Å) which has been atomistically modeled.[9] Both gas solubility and self-diffusivity in the confined IL are compared against the values in the bulk IL. Additionally, the self-diffusivity values for the confined IL and the bulk IL are also compared with each other at low and high temperatures. The CO_2, H_2, N_2, and H_2O were studied because these gases represent the major gas components from which CO_2 is captured. Simulation results are also compared with available experimental data for similar confined IL systems.

2 Theory and simulation methods

2.1 $NP_{xy}T$ ensemble

The $NP_{xy}T$ ensemble (constant number of particles, constant *xy*-component pressure tensors, and constant temperature) has been used to compute the density of the pure [hmim][Tf_2N] confined into 2-D silica slit pores. In this ensemble, the fundamental thermodynamic equation describing a system of N pairs of cations and anions adsorbed inside a slit pore is given by

$$dG = -SdT + \mu dN + T_{zz}AdH - Ad(T_{xy}H) \tag{1}$$

where $G = \mu N$ is the Gibbs free energy, μ is the chemical potential for the adsorbate (the adsorbed IL), T is the temperature, S is the entropy, H is the slit pore width, A is the area for the wall, T_{zz} and T_{xy} are the stresses in the directions perpendicular and parallel to the walls, and they are equal to the negative values of the corresponding pressure tensor components. By specifying values for T, N, H, $T_{xy} = -P_{xy}$ variables, the $NP_{xy}T$ Monte Carlo (MC) simulations were performed to compute the average molar volume for confined IL. The acceptance rules for the $NP_{xy}T$ ensemble are very similar to those used in the generic NPT MC simulations, except for the change of area A (refer to Supporting Information for details), rather than volume as in the NPT ensemble.

2.2 Isostress-osmotic ($N_2P_{xy}Tf_1$) ensemble

We have used the isostress-osmotic ensemble to calculate the amounts of gas absorption in confined IL. The isostress-osmotic ensemble is a combination of the grand-isostress[10] and the osmotic ensemble.[11] The fundamental thermodynamic equation for the isostress-osmotic ensemble is given by

$$dG_2 = -SdT - N_1 d\mu_1 + T_{zz} A dH - Ad(T_{xy} H) + \mu_2 dN_2, \tag{2}$$

where $G_2 = \mu_2 N_2$. 1 and 2 denote the gas solute and the IL solvent molecules, respectively. The meaning of the other symbols in Equation (2) is the same as in Equation (1). By specifying T, μ_1 (f_1), T_{xy} ($-P_{xy}$), N_2, and H, where f_1 is the fugacity for the gas solute, isostress-osmotic MC simulations were performed. Note that the pressure tensor component P_{xy} was set to be equal to the bulk gas pressure. Implementations for the isostress-osmotic ensemble are similar to those for the osmotic ensemble, in which T, f_1, P, N_2 are specified.[12] The only difference is that the pressure P in the osmotic ensemble is replaced by the pressure tensor components P_{xy} in the isostress-osmotic ensemble. Additionally, in the isostress-osmotic ensemble, it is also necessary to specify the slit pore width H.

The continuous fractional component (CFC) method[12,13] was used to insert and delete gas solute molecules in the isostress-osmotic ensemble. The acceptance rules in the CFC isostress-

osmotic MC ensemble are very similar to those for the CFC osmotic ensemble.[12] Specifically, in the isostress-osmotic MC simulations there are three types of moves, i.e., the thermal move, the area A move, and the λ move, where λ is the coupling strength between the fractional gas solute molecule and the other solute and solvent molecules. Details about this method can be found in our previous work.[12,14,15] In simulations the interaction between the fractional gas solute molecule and the silica wall was not scaled. Instead, when an attempt was made to insert a fractional gas solute molecule inside the slit pore at a position separated by less than 0.5 Å from the wall, the attempted insertion was simply rejected and the old configuration was collected for sampling and property calculations.

2.3 Simulation details

2.3.1 Classical force field

A classical force field has been used to simulate IL, gas solutes, IL-gas, and the adsorbate (gas, IL)-adsorbent interactions. The interaction energy for the system is given by,

$$\begin{aligned}
\mathscr{V}(\mathbf{r}) &= \sum_{\text{bonds}} k_b(r-r_0)^2 + \sum_{\text{angles}} k_\theta(\theta-\theta_0)^2 \\
&+ \sum_{\text{dihedrals}} k_\chi[1+\cos(n_0\chi-\delta_0)] + \sum_{\text{impropers}} k_\psi(\psi-\psi_0)^2 \\
&+ \sum_{i=1}^{N-1}\sum_{j=i+1}^{N}\left\{4\varepsilon_{ij}\left[\left(\frac{\sigma_{ij}}{r_{ij}}\right)^{12}-\left(\frac{\sigma_{ij}}{r_{ij}}\right)^{6}\right]+\frac{q_iq_j}{r_{ij}}\right\} \\
&+ U_{sf}, \qquad (3)
\end{aligned}$$

where the symbols have their conventional meaning,[16] U_{sf} describes the interaction between adsorbates and two opposite silica walls.

The U_{sf} was computed using two models, i.e., the smooth and atomistic potential models. The smooth potential model was used in our in-house MC and molecular dynamics (MD) software. In MD simulations using the smooth potential, a simple reflection from the wall (reflective boundary conditions) rather than randomizing velocities of particles after repulsion from the wall (diffusive

boundary conditions)[17] was used. The adsorbate atom interactions in a slit pore with two walls were calculated as $U_{sf} = \phi_{\rm sf}(z) + \phi_{\rm sf}(H-z)$, and $\phi_{\rm sf}(z)$ is given by the 9-3 potential[18]

$$\phi_{\rm sf}(z) = \frac{2\pi\rho_s\sigma_{\rm sf}^3\varepsilon_{\rm sf}}{3}\left[\frac{2}{15}(\frac{\sigma_{\rm sf}}{z})^9 - (\frac{\sigma_{\rm sf}}{z})^3\right], \tag{4}$$

where z is the distance between the atom and the wall, and ρ_s is the silica number density. Cross-parameters $\sigma_{\rm sf}$ and $\varepsilon_{\rm sf}$ were calculated from the standard Lorentz-Berthelot mixing rules. The parameters for silica are: $\sigma_s = 3.0$ Å, $\varepsilon_s = 0.8$ kJ/mol, and $4\pi\rho_s = 0.5/\text{Å}^3$.[19]

In MD simulations using the NAMD program,[20] the atomistic silica potential model was used to obtain more realistic estimates for the self-diffusivity values. The U_{sf} was calculated by explicitly summing all the Lennard-Jones (LJ) and electrostatic (ELEC) interactions between the adsorbates and the Si and O atoms of the silica wall. The Si and O atom positions were fixed during simulations by using the *fixedAtoms* utility provided in the NAMD program. The charges and LJ parameters for Si and O atoms in the silica structure were developed in this work (see Result Section). Two atomistic silica slit pores (25 Å and 45 Å) were constructed. Each silica pore consists of two slabs and contains 980 Si atoms and 1960 O atoms on the two opposite walls. The silica wall has a dimension of 45.99 Å$\times$ 45.99 Å in the *xy*-plane parallel to the silica walls. The thickness for each silica slab is about 7.7 Å. The procedure to construct silica slit pores is described in detail in the Supporting Information. In this work, we have not investigated the surface chemistry such as the surface hydroxylation of the silica.

In CFC MC simulations, the LJ parameters for the fractional molecule were scaled using a functional form proposed by van Gunstern *et al.*[21] to aid insertion when computing the interaction between the fractional molecule and other adsorbate molecules. A switching function was turned on at 10.5 Å and turned off at 12.0 Å for the LJ potential. A Verlet neighbor list with a 13.5 Å radius was used. The intra-molecular ELEC and LJ interactions for atoms separated by exactly three consecutive bonds were scaled by 0.5 and were neglected for atoms separated by less than three consecutive bonds. The classical force field parameters for H_2O, CO_2, N_2, H_2, $[Tf_2N]^-$ anion, and

[hmim]$^+$ cation were obtained from previous work.[15,22,23] To evaluate the accuracy of the force field for [hmim][Tf_2N], the simulated densities for the IL were compared with the experimental values. At 313 and 373 K, the simulated densities are only 0.1-0.3% different than the experimental values.[24] At 423 K and 400 bar, the simulated density agrees with the experimental value[25] within the simulation uncertainty. At 573 K, there is no experimental density for comparison. The experimental densities in the temperature range 313-373 K[24] were linearly extrapolated to 573 K. The simulated density at 573 K is 2.3% different than the experimental extrapolation value. The force field parameters for the IL satisfactorily reproduce the experimental densities at 313-573 K. The Fennel and Gezelter shift force (FGSF)[26] method was used to speed up the calculation of the ELEC interaction in MC simulations. A cutoff value of 12.0 Å and a damping parameter $\kappa = 0.2022$ Å^{-1} were chosen in the FGSF method. The FGSF method was also validated against the standard Ewald method in this work (Supporting Information). In MD simulations, the standard Ewald method was used in the locally developed MD code and, the Particle Mesh Ewald (PME) method was used in NAMD program to compute the ELEC interactions. In this work, a pseudo-2D was applied to calculate ELEC interactions in the Ewald type and FGSF methods by using a large simulation box size in the z direction compared to the silica slit pore width.

2.3.2 Monte Carlo simulations

The $NP_{xy}T$ simulations were performed with a pressure tensor P_{xy} of 1 bar and in the temperature range 313-573 K for 60 pairs of [hmim]$^+$ cations and [Tf_2N]$^-$ anions confined in silica slit pores (25-45 Å). The simulation box size in the z direction was set to be 50-60 Å to minimize the interaction between adsorbate molecules in the primary cell and image cells. Simulations included several million steps of equilibration followed by about 20 million steps of production runs. During the equilibration various MC moves were tuned to achieve roughly 50% acceptance rates.[4] These moves were: thermal equilibration via hybrid Monte Carlo[4,15,27] (HMC) (90%) and area A changes (10%). The values in parentheses represent the fixed probabilities during the run.

In the $N_2P_{xy}Tf_1$ simulations, the number of IL molecules was set to be 60 pairs. For CO_2,

the temperatures and pressure tensors were set to be in the range of 333−573 K and 4-83.6 bar. For H_2, the temperatures and the pressure tensors were 313−573 K and 50−300 bar. For N_2, the temperatures and pressure tensors were 298-333 K and 40-500 bar. In the case of H_2O, the temperature was set to be 373 K and the pressure tensors were 0.05-0.2 bar. Equilibration runs of typically 2 million moves were carried out during which various MC moves were tuned to achieve roughly 50% acceptance rates. These moves were: thermal equilibration via HMC (40%), λ move (50%), and area A move (10%). Production runs of about 20 million steps were typically used. The CFC bias factor[12] was adjusted during the equilibration stage to achieve as closely as possible a uniform probability distribution of λ. Optimization of these bias factors was done using the Wang-Landau[28] updating scheme. The gas fugacity f_1 was calculated from the Peng-Robinson equation of state[15] for CO_2, N_2, and H_2O and, from MD simulations for H_2.[23] Note that P_{xy} was set to be equal to the pressure in the gas phase.

The CFC grand canonical[12] MC simulations were performed to compute CO_2, H_2, N_2, and H_2O adsorption into 25-45 Å empty silica slit pores (without confined ILs) at similar same temperatures and pressures to those used in the $N_2P_{zz}Tf_1$ simulations. Simulation details in this case were very similar to those for $N_2P_{zz}Tf_1$ except that there was no A move in the grand canonical ensemble. The slab wall lengths in the x and y directions were set to be 40-200 Å.

2.3.3 Molecular dynamics simulations

Molecular dynamics simulations in the NVT and NVE ensembles were performed using both the in-house software in the case of smooth silica potential, and the NAMD program[20] when the atomistic silica potential was used. The time step was 0.5-1.0 fs. Simulations were performed for 60-155 [hmim][Tf_2N] ILs confined in 25-45Å silica slit pores. The densities for the confined IL in MD simulations were obtained from $NP_{xy}T$ MC simulations at P_{xy} of 1 bar. Simulations were typically carried out for 5 ns of equilibration followed by 10 ns production runs. The self-diffusivity in the xy directions was calculated from the NVE MD trajectories using a procedure

similar to the one described previously[23,29]

$$D_{\text{self},xy} = \lim_{t\to\infty} \frac{1}{4t} < |x(t) - x(0)|^2 + |y(t) - y(0)|^2 > . \quad (5)$$

Self-diffusivities were calculated using both the smooth and the atomistic silica potential models. Most of the results below were obtained using the smooth silica potential model unless the atomistic silica potential model was explicitly indicated for use in simulations.

Note that in a binary mixture consisting of A and B, the self-diffusion coefficients for A and B are defined as the diffusion coefficients for the individual label molecules A*, and B*, i.e., D_{A*}, D_{B*}, when there is no concentration gradient of (A+A*) or (B+B*).[30] In experiments, $D_{A}*$, D_{B*} can be measured by the use of isotopes. In simulations, the self-diffusion coefficients D_{A*}, D_{B*} are calculated from the mean squared displacement of A and B,[31] which is also consistent with the definition of self-diffusivity in mixtures.

3 Results and discussion

3.1 Solid-fluid interaction

The interaction between the C atom of CO_2 and the silica slit pore, graphite slit pore, and CNT were obtained using the 9-3 potential for graphite[32] and silica pores, and the atomistic potential for the CNT,[4] respectively. The results are shown in Figure S2. In the case of slit pores, two well depths are positioned close to the walls. The well depths are the same for the 25 Å, 35 Å, and 45 Å silica slit pores, and they are about 1.8 and 4 times smaller than for the graphite slit pore and the (20,20) CNT, respectively. All other atoms such as the O atom in CO_2, the F, O, S, C, and N atoms in the $[Tf_2N]^-$ anion, and the H, N, and C atoms in the $[hmim]^+$ cation exhibit the same behavior. The adsorbate atom interactions with the 25 Å silica slit pore are about two and four times weaker than with the 25 Å graphite slit pore and the (20,20) CNT, respectively.

3.2 Thermodynamic properties for pure [hmim][T_2N] confined in silica slit pores

3.2.1 Molar volume and density for [hmim][Tf_2N] confined in silica slit pores

Since molar volume is important to determine gas solubility in ILs,[23] the molar volume and density for confined [hmim][Tf_2N] were calculated and the results are shown in Table 1 and Figure S3. Note that different sets of simulations starting from different initial configurations have been run with the same temperatures and pressure tensors; the molar volumes among these different simulations vary by only 1.7%. This result implies that the simulations are long enough to obtain good estimates of the molar volume and density for the confined IL.

The densities for [hmim][Tf_2N] confined in silica slit pores are smaller than the ones for the bulk IL. In silica slit pores with pore widths between 25 Å and 45 Å, the confined IL exhibits a 12-31% smaller density than the bulk IL at 313-573 K and 1 bar. The density for the confined IL increases when the slit pore width is increased. For example, when the pore width is increased from 25 Å to 35 Å, the density for the confined IL increased by 7-11%. When the pore width is further increased from 35 Å to 45 Å, the confined IL is more densely packed. As the silica pore becomes larger and larger, the density for the confined IL is expected to approach the value for the bulk IL. Interestingly, the IL in the (20,20) CNT exhibits a smaller density than that in the 25 Å-wide silica slit pore.

3.2.2 Structure of [hmim][Tf_2N] confined in silica slit pores

The local density for the center of mass of the confined IL in silica slit pores was also calculated, and the local density profiles are shown in Figure 1 and Figure S4. In the 25 Å-wide silica slit pore, the $[hmim]^+$ cation exhibits two layers at about $z = \pm 5$ Å. The distance between the two neighboring $[hmim]^+$ layers is about 10 Å. The $[Tf_2N]^-$ anion exhibits three layers. Two layers are positioned at $z = \pm 7$ Å, and the third layer occurs at the center. The distance between the two neighboring $[Tf_2N]^-$ layers is about 7 Å. The confined IL exhibits smaller local density than

the bulk IL in certain regions. For example, in three regions of -12.5 Å$\leq z \leq -6.5$ Å, -2.0 Å$\leq z \leq 3.0$ Å, and 6.8 Å$\leq z \leq 12.5$ Å, the confined [hmim]$^+$ exhibits smaller local density than the bulk. It is due to the smaller local IL densities in these regions that lead to smaller overall density for the confined IL compared to the bulk IL (Figure S3).

In the case of 35 Å-wide silica slit pore, there are four cation layers; the distance between the neighboring [hmim]$^+$ layers was estimated to be 7.5 Å (Figure 1). Five layers of [Tf_2N]$^-$ occur and the distance between the neighboring anion layers is about 6 Å (Figure S4). The distances between the neighboring cation/anion layers in the 35 Å-wide slit pore are smaller than in the 25 Å-wide slit pore. This arrangement leads to a more densely packed IL structure and larger densities for the confined IL in the 35 Å-wide slit pore compared to the 25 Å-wide slit pore. Note that the peak heights in the 25 Å and 35 Å-wide slit pores are similar. This similarity is partly due to the same solid-fluid potential well depth for the 25 Å and 35Å-wide silica slit pores (Figure S2).

The density peak heights for the cation/anion layers in the silica slit pores are 2-3 times smaller than in the regions close to the (20,20) CNT wall. This result is consistent with the stronger fluid interactions with the (20,20) CNT compared with the silica slit pores (Figure S2). Finally, note that the density profiles for IL in silica slit pores (Figure 1 and Figure S4) are not smooth nor completely symmetric relative to the center plane ($z = 0$). This indicates that longer simulations are required to get better statistics.

3.2.3 Interaction energies

In addition to the density, the interactions between the IL molecules themselves, and between the IL and the silica slit pores have been calculated. The corresponding results are shown in Table S3. The bonded energy values U_{IL}^{b} for the bulk and confined IL are similar, suggesting that the intramolecular configurations for the bulk and confined IL are also similar. The non-bonded energy U_{IL}^{nb} for the confined [hmim][Tf_2N] in the (20,20) CNT is weaker than in the silica slit pores, which is in turn weaker than the U_{IL}^{nb} for the bulk IL. This observation is consistent with the smaller density for confined IL in the (20,20) CNT relative to the silica slit pores and the fact

that the bulk IL exhibits the highest density (Figure S3). The solid-fluid interaction energy U_{sf}^{nb} between the silica slit pore and the IL becomes weaker when the slit pore width is increased; it changes from -8.19 kJ/mol in the 25 Å -wide pore to -4.23 kJ/mol in the 45Å -wide pore. The IL interaction with the (20,20) CNT is about 62 kJ/mol stronger than with the 25Å -wide silica slit pore (Table S3) which is consistent with the stronger solid-fluid potential for the (20,20) CNT than for the silica pores (Figure S2).

The total non-bonded energy U_t^{nb} for the bulk IL is 5-12 kJ/mol greater than that of the IL confined in silica slit pores, and 30 kJ/mol smaller than that of the IL confined in the (20,20) CNT, respectively. These findings are consistent with the experimental observations that melting temperatures for ILs decrease when ILs are confined in silica pores,[33–35] but increase when ILs are confined in the CNT.[36] It is expected that the melting temperature will decrease when the non-bonded interaction U_t^{nb} becomes weaker.

3.3 Thermodynamic properties for CO_2, N_2, H_2, and H_2O absorption in confined [hmim][Tf_2N]

3.3.1 Solubility of gases in confined [hmim][Tf_2N]

The calculated gas solubilities for CO_2, H_2, N_2, and H_2O in silica confined [hmim][Tf_2N] are summarized in Table S2. The CO_2 solubilities in IL confined in a silica pore of 25 Å width are about 1.1-1.7 times larger than those in the bulk IL[15] at 333-573 K and 4-83.6 bar (Figure S5). In larger silica pores, CO_2 solubilities in the confined IL are still typically larger than in the bulk IL. For example, CO_2 solubilities in IL confined in the 35-Å -wide silica pore are 20-25% larger than in bulk IL at 333 K and 4-17.15 bar. In the 45 Å -wide silica slit pore, CO_2 solubility in the confined IL is about 10% larger than in the bulk IL at 333 K and 8 bar. As shown in Figure S5, it appears that CO_2 in the bulk IL generally shows a linear relationship between pressure and CO_2 solubility, but the confined IL is noticeably non-linear, especially at high pressures. When CO_2 molecules are absorbed in the IL, the cations and anions will adjust themselves to allow for

more free volume for CO_2 molecules to fit in. Under the confinement, this adjustment is restricted by silica walls. Consequently, CO_2 solubility in the confined IL versus pressure is non-linear and approaches a plateau-like region compared to the bulk IL. For H_2, gas solubilities in confined IL in silica pores of 25-45 Å are 1.2-2.3 times larger than in the bulk IL[23] at 313-573 K and 50-300 bar. Similarly, N_2 solubilities in confined IL in a 25-Å -wide silica slit pore are 1.8-3.4 times larger than in the bulk IL[22] at 298-333 K and 40-500 bar. In contrast, water solubilities in the confined and bulk ILs[15] are comparable with an average difference of about 10% at 373 K in a 25-Å -silica slit pore.

When the silica slit pore width is increased, CO_2 and H_2 solubilities in confined [hmim][Tf_2N] typically decreases (Table S2). For example, when the silica slit pore width is increased from 25 Å to 35 Å, CO_2 solubilities decrease by about 20% at 333 K and 4-17 bar; H_2 solubilities decrease by about 30-45% at 313 K and 50-300 bar. When the silica slit pore width is further increased from 35 Å to 45 Å, CO_2 solubilities decrease by 10-20% at 333 K and 4-17 bar; H_2 solubility decreases by about 15% at 313 K and 100 bar. In larger silica slit pores, confined [hmim][Tf_2N] exhibits smaller molar volume (Figure S3). This decrease results in smaller solubilities for CO_2 and H_2 in IL confined in larger silica pores.

When the temperature is increased from 333 K to 573 K, CO_2 solubility in confined [hmim][Tf_2N] decreases (Table S2 and Figure S5). In contrast, H_2 solubility in the confined IL increases. Similar to CO_2, N_2 solubility in confined [hmim][Tf_2N] also decreases with temperature from 298 K to 333 K. These temperature effects on the solubility of CO_2, H_2, and N_2 in confined [hmim][Tf_2] are the same as in the bulk IL.[22,23] From gas solubility at different temperatures, the CO_2 heat of absorption in the 25 Å -silica-pore confined [hmim][Tf_2N] was estimated to be 10.6 ± 1.4 kJ/mol, very close to the value of 10.3 kJ/mol for CO_2 in the bulk IL.[15]

The interactions of CO_2, H_2, and N_2 with [hmim][Tf_2N] are weaker than the H_2O-[hmim][Tf_2N] interaction. For example, ab initio calculations show that CO_2 interaction energies are about -17 kJ/mol and -22 kJ/mol with the $[hmim]^+$ cation and $[Tf_2N]^-$ anion, respectively. These interaction energies are much weaker than the corresponding H_2O interaction energies of -43 kJ/mol

with both the $[hmim]^+$ cation[37] and $[Tf_2N]^-$ anion through hydrogen-bonding. For CO_2, H_2, and N_2, the IL molar volume is important to determine the gas solubility due to their weak interaction with [hmim][Tf_2N] compared to the water-[hmim][Tf_2N] interaction. The silica-confined [hmim][Tf_2N] exhibits larger molar volumes than the bulk IL (Figure S3). Hence, the solubilities of CO_2, H_2, and N_2 in the silica-confined IL are 1.1-3.4 times larger than in the bulk IL. As shown in Figure S3, [hmim][Tf_2N] confined in silica slit pores exhibits much smaller molar volume than [hmim][Tf_2N] confined in a (20,20) CNT. Additionally, the fluid interaction with the (20,20) CNT is stronger than with the silica pores (Figure S2). Hence, CO_2 and H_2 solubilities in the 25 Å -silica-confined [hmim][Tf_2N] are 1.2-4 times smaller than in the (20,20)-CNT-confined IL at 313-573 K and 4-200 bar.[4] In the case of water, the molar volume of the IL plays a less important role in determining water solubility. Hence, steam water solubilities in silica-confined [hmim][Tf_2N] are only 10% different from the solubility values in the bulk IL.

The calculated CO_2 solubilities in silica-confined [hmim][Tf_2N] were compared with available experimental data for similar system. Recently, Deng and colleagues[38] have experimentally determined that when [bmim][BF_4] is confined in silica gel pores of 30-120 Å width CO_2 solubilities in the confined [bmim][BF_4] are 1.5 times larger than in the corresponding IL simply coated on the silica gel surface. Their experimental data suggest that CO_2 solubility in the silica-confined IL is larger than in the bulk IL, which is consistent with our simulations.

Finally, the degree of gas adsorption in empty silica slit pores was calculated (Table S1) and compared with the gas solubilities in silica-confined [hmim][Tf_2N]. The H_2 solubilities in the confined IL are 4-13 times smaller than in the empty silica pores (25Å-45Å) at 313-573 K and 50-100 bar. The N_2 solubilities in the confined IL are 4-7 times smaller than in the empty silica pore (25 Å) at 298-333 K and 50-500 bar. The larger amounts of H_2 and N_2 adsorbed in the empty silica pores compared to the confined IL are due to the larger void space (free volume) in the empty silica pores. For water, the confined IL exhibits about 40 times more gas solubility than the empty silica pore (25 Å) at 373 K and 0.05-0.2 bar. This increase is due to the much stronger water interaction with [hmim][Tf_2N] (Figure S6) compared to the silica pore. The CO_2 solubility

exhibits complicated behavior. At a low temperature of 333 K and pressures of 4-17.15 bar, CO_2 solubilities in the confined IL are 1.4-2.0 times larger than in the empty silica pores (25 Å-45Å). However, at high temperatures of 423-573 K and pressures of 8-83.6 bar, CO_2 solubilities in the confined IL are 1.2-1.9 times smaller than in the empty silica pore (25 Å).

3.3.2 Structures of gases and confined IL

Three representative snap shots for CO_2, H_2 and H_2O absorption in confined [hmim][Tf_2N] are shown in Figure 2. Gases absorption into confined IL is complex. One could envision a competition between absorption (in IL volume) and adsorption (on the silica surface). At low gases concentrations, most H_2 molecules are positioned in the regions near the silica walls. In the case of CO_2, some CO_2 molecules are absorbed in the regions near the wall and several other CO_2 molecules are absorbed inside the IL (Figure 2 and Figure 3). Most N_2 molecules also occupy the regions near the wall at low gas solubilities (not shown). In contrast, water molecules are located inside the IL region rather than near the silica walls. This arrangement is due to the strong hydrogen-bonding interactions between water and [hmim][Tf_2N] (Figure S6). The corresponding local density distributions of the center-of-mass for CO_2, H_2, N_2, and H_2O absorption in [hmim][Tf_2N] confined in a silica pore (25 Å) are shown in Figure 3.

3.4 Self-diffusivity

3.4.1 Self-diffusivities for gases in confined [hmim][Tf_2N] using the smooth silica potential model

The solid-fluid interaction energy in the smooth potential model only depends on z (Equation 4), resulting in no net force in the xy-plane for the adsorbate molecules. Therefore, the center of mass (CM) for all the adsorbate molecules (IL + gas) was moved to the same origin in the xy-plane when the mean squared displacement (MSD) was calculated. The MSD values in the xy-plane for the CM of CO_2, H_2, and N_2 gases at 8 mol% in the silica-pore (25 Å) confined [hmim][Tf_2N] are

shown in Figure 4. The MSD values for CO_2, H_2, and N_2 in the confined IL are much larger than in the corresponding bulk IL at 298-573 K. Gas self-diffusivity in the confined IL was calculated from the MSD value,[23] and the results are summarized in Table 2. The CO_2 self-diffusivity values in the confined IL are 2.4-8.3 times larger than in the bulk IL at 313-573 K. The H_2 self-diffusivities in the confined IL are 3.7-4.5 times larger than in the bulk IL at 313-573 K. The N_2 self-diffusivities in the confined IL are 3.4-5.3 times larger than in the bulk IL at 298-373 K. Note that most $\beta = d(log\Delta r^2)/d(logt)$ values for all gases are close to 1 (Table 2), indicating that 10-ns NVE simulations are long enough to obtain gas normal diffusion.

The enhanced gas self-diffusivity values for CO_2, H_2, and N_2 gases in the confined [hmim][Tf_2N] compared to the bulk IL are likely associated with these gases being mainly absorbed in the regions close to the silica wall where the IL density is very low (Figure 3 (a), (b), (c)). It is expected that these gas molecules will experience far less frequent collisions with the IL molecules near the silica wall than in the bulk IL, which leads to larger self-diffusivity values for these gases in the silica-confined IL. Similarly, it has been shown that the self-diffusivity coefficients for the CO_2 and H_2 gases in the CNT-confined [hmim][Tf_2N] are much larger than in the bulk IL,[4] partly due to these gases mainly being positioned close to the CNT tube wall where the IL exhibits very low density (not shown here).

In contrast, water in confined [hmim][Tf_2N] exhibits diffusion behavior very different than CO_2, H_2, and N_2 gases. As shown in Figure S7, at 298 K water in the confined IL exhibits MSD values much larger than in the bulk IL, leading to the self-diffusivity for water in the confined IL being 1.8 times larger than in the bulk IL (Table 2). However, the MSD values for water in the confined and bulk ILs are comparable to each other at a higher temperature of 373 K. As discussed above (Figure 3 (d)), water exhibits the largest density inside the IL region where the IL density is also high. Hence, unlike CO_2, H_2, and N_2 gases, the enhanced water self-diffusivity in the confined IL at 298 K can not be ascribed to the density distribution profiles for water and the confined IL. Water molecule forms hydrogen bonds with both the $[hmim]^+$ cations and the $[Tf_2N]^-$ anions (Figure S6) coupling the diffusivities of water and the IL. As shown below, confined [hmim][Tf_2N]

diffuses faster than the bulk IL at 298 K and as a result increases the self-diffusivity of water in the confined IL compared to the bulk IL.

3.4.2 Self-diffusivity for confined [hmim][Tf_2N] using the smooth silica potential model

The MSD values in the *xy*-plane for the $[hmim]^+$ cation and $[Tf_2N]^-$ anion confined in the silica slit pore (25 Å) are shown in Figure S8. At a lower temperature of 298 K, the confined IL exhibits a larger MSD value (Figure S8 (a)) and 1.7 times larger self-diffusivity than the bulk IL. In contrast, at a higher temperature of 373 K, the confined IL exhibits a smaller MSD value (Figure S8 (b)) and 1.4-1.7 times smaller self-diffusivity than the bulk IL. At an intermediate temperature of 313 K, the MSD and self-diffusivity values for the confined IL are similar to those for the bulk IL. The enhanced self-diffusivity for the confined IL at 298 K is consistent with other simulations. Hung and colleagues demonstrated that the IL molecules in the center of a graphite slit pore could diffuse faster than those in the bulk IL.[6]

A similar temperature-dependent confinement effect on IL self-diffusivity has also been obtained from the experimental work by Iocab et al.[7] At 182 K, confined [bmim][BF_4] in a silica nanopore (104 Å) diffuses faster than the corresponding bulk IL. However, when the temperature is increased to about 250 K, the bulk IL diffuses faster than the confined IL. Silica pore confined [hmim][Tf_2N] exhibits a larger molar volume and smaller density (Figure S3) than the bulk IL, and in some regions the local density for the confined IL is smaller compared to the bulk IL (Figure 1 and Figure S4). The IL molecules in the low density regions are expected to diffuse faster than in the bulk IL. This local increase in diffusivity leads to enhanced overall diffusivity for the confined IL at low temperatures. On the other hand, the silica wall retards IL movement, and this reduction in mobility may be responsible for the decrease in self-diffusivity for the confined IL at high temperatures. More studies are needed to fully understand the temperature role in the self-diffusivity for the confined IL.

3.4.3 Self-diffusivities for CO_2 and confined [hmim][Tf_2N] using the atomistic silica potential model

All the above self-diffusivity values for the confined IL and gases were calculated using a smooth silica potential model (Equation 4). It is important to determine whether the atomistic and smooth silica potential models give similar self-diffusivity results for the confined IL and gas.

In the atomistic silica potential model, the van der Waals (VDW) parameters and charges for the Si and O atoms from Schulten[39] were tuned in this work to give CO_2 adsorption in the silica slit pore (25 Å) consistent with those values obtained from the smooth silica potential model. The VDW parameters and charges for Si and O atoms were chosen to be: $\varepsilon_{Si} = 0.0375$ kcal/mol, $\sigma_{Si} = 3.826$ Å, $q_{Si} = 0.1$; $\varepsilon_O = 0.01875$ kcal/mol, $\sigma_O = 3.118$ Å, $q_O = -0.05$. Note that the *xyz* coordinates for Si and O atoms for the silica slit pore (Figure S9) in the atomistic model were fixed during simulations. These atomistic force field parameters for the Si and O atoms give CO_2 adsorption 8-15% different than the smooth silica potential model at 333-423 K and 8-17.15 bar (Table S4), a satisfactory level of agreement.

Local density distributions using the atomistic silica potential model Local density distributions for gas and IL molecules were calculated because they are important to determine self-diffusivities. The density profiles are shown in Figure S10. Overall, the atomistic and smooth potential models give similar local density distributions for $[hmim]^+$ cations, $[Tf_2N]^-$ anions, and CO_2 molecules. Similar to the smooth silica potential model, the atomistic silica model also predicts that CO_2 molecules exhibit the highest peak density close to the silica walls where the IL density is low. This result is consistent with the simulated snap shot (Figure S9).

Self-diffusivities using the atomistic silica potential model The atomistic silica model gives CO_2 self-diffusivities (Table S5) only 3-10% different than the smooth silica model. The CO_2 self-diffusivity coefficients from the atomistic silica model in the confined IL are 7.5 and 2.5 times larger than in the bulk IL at 313 K and 373 K, respectively. This difference is also partly due to

CO_2 absorption close to the silica wall (Figure S10). When computing self-diffusivities, the center of mass for the IL and CO_2 molecules was not moved to the same origin because the net forces in the *xy*-plane due to atomistic silica walls on adsorbate molecules are not necessarily zero. Most $\beta = d(log\Delta r^2)/d(logt)$ values for CO_2 and the confined IL are close to 1 (Table S5), suggesting that 10-ns NVE simulations are long to obtain normal diffusion for both gas and the IL.

The MSD values in the *xy*-plane for confined [hmim][Tf_2N] in a 25 Å silica pore are shown in Figure S11, and the corresponding self-diffusivities are summarized in Table S5. At 313 K, the atomistic silica potential model gives much larger MSD values for the confined IL than the smooth silica potential model even though the local density distributions are similar for both models (Figure S10). At a higher temperature of 373 K, the atomistic silica model gives slightly larger MSD values than the smooth silica potential model. These results suggest that the atomistic silica model has a more significant effect on IL dynamics than on IL structure, especially at low temperatures. Despite the MSD difference between the two silica models, the atomistic silica model also predicts that the confined IL exhibits larger self-diffusivity at lower temperatures and smaller self-diffusivity at higher temperatures compared with the bulk IL. At a lower temperature of 313 K, the self-diffusivity for the confined IL obtained from the atomistic silica model is 4.7 times larger than for the bulk IL. However, at 373 K, the self-diffusivity for the confined IL from the atomistic silica model is 1.3 times smaller compared to the bulk IL.

3.4.4 Silica slit pore size effects on self-diffusivity

Self-diffusivities for CO_2 and [hmim][Tf_2N] confined in a larger silica slit pore (45 Å) were also calculated using the atomistic silica potential model and compared with the results in a smaller silica pore (25 Å). As shown in Table S5, CO_2 self-diffusivities in the 45 Å-pore confined IL at 313-373 K are 30-43% smaller than in the 25 Å-pore confined IL, but still 1.8-4.3 times larger than CO_2 diffusivity coefficients in the corresponding bulk IL. The behavior of self-diffusivity coefficients for the confined IL in different pores as a function of temperature within the range of 313-373 K are complex. At 313 K, the self-diffusivity for the confined IL in the 45 Å-pore is close

to the value in the 25 Å-pore and five times larger than the diffusivity for the bulk IL. However, at 373 K the self-diffusivity for the confined IL in the 45 Å-pore is 3.3 times larger than in the 25 Å-pore and 2.7 times larger than the diffusivity value for the bulk IL.

3.4.5 Silica force field parameter effects on self-diffusivity

Finally, the effects of the force field parameters for Si and O atoms on self-diffusivity were examined. When the ε values for Si and O atoms in the atomistic silica model were increased eight times leading to stronger solid-fluid interactions, the CO_2 self-diffusivity at 313 K in the confined IL (25 Å pore) decreased by 22% but remained 5.8 times larger than CO_2 diffusivity in the bulk IL. Additionally, the CO_2 adsorption in an empty silica slit pore (25 Å) was found to increase 6.4 times. In contrast, the self-diffusivity for the confined IL at 313 K decreases by a factor of 32, becoming 7.5 times smaller than the diffusivity for the bulk IL. These findings strongly suggest that the force field parameters for Si and O atoms affect the self-diffusivity for CO_2 in a small but significant way for the confined IL. It is interesting to note that all simulations in this work show that the self-diffusivity for CO_2 in the confined IL is much larger than in the bulk IL whether or not the confined IL diffusivity is larger or smaller than the bulk IL.

4 Conclusions

Monte Carlo and molecular dynamics simulations were implemented to study pure [hmim][Tf_2N] confined in silica slit pores (25-45 Å). Absorption of gaseous CO_2, H_2, N_2, and H_2O in the confined IL were also examined, and self-diffusivity coefficients for both the gases and IL molecules were determined.

Silica-confined [hmim][Tf_2N] exhibits 12-31% smaller density than the corresponding bulk IL at 313-573 K and 1 bar. Several cation and anion layers occur in silica slit pores, and these layers exhibit peak density about two times larger than the bulk IL. Non-bonded interaction energy for bulk [hmim][Tf_2N] is about 5-12 kJ/mol larger compared to the silica-pore confined IL but

30 kJ/mol smaller compared to the (20,20)-CNT confined IL. These values are consistent with increased melting temperatures for the CNT-confined IL[36] and decreased melting temperatures for the silica-pore confined IL.[33–35]

For gases which interact weakly with IL molecules, the molar volume for the confined IL is important to determine their solubilities. Larger molar volumes for the confined IL leads to solubilities for weakly absorbing gases such as CO_2, H_2, and N_2 in the silica-pore confined [hmim][Tf_2N] which are 1.1-3 times larger than those in the bulk IL at 298-573 K. This increase is consistent with experimental findings showing CO_2 solubility in silica-pore confined [bmim][BF_4] is larger than in the corresponding bulk IL.[38] However, for water which interacts strongly with the [hmim][Tf_2N] through water-IL hydrogen bonding interactions, the molar volume for the confined IL is less important in determining water solubility. Water solubilities in silica-pore confined and bulk [hmim][Tf_2N] were found to be similar with a variability of less than 10%.

Simulations show that silica-pore confined [hmim][Tf_2N] exhibits larger self-diffusivity at 298 K but smaller self-diffusivity at 373 K than the corresponding bulk IL. This result is consistent with the experimental findings by Iocab et al.[7] that silica-pore confined [bmim][BF_4] exhibits much larger self-diffusivity at 182 K but smaller self-diffusivity at 250 K compared to the bulk IL.

The self-diffusivity for weakly absorbing gases such as CO_2, H_2, and N_2 in silica-pore (25 Å) confined [hmim][Tf_2N] were found to be 2.4-8.3 times larger than in the bulk IL at 298-573 K. This trend arises because these gases are most likely to be absorbed close to the silica walls where the IL density is very low. Due to both higher CO_2 solubility and larger CO_2 self-diffusivity in the confined IL compared with the bulk, CO_2 permeability in the silica-pore confined [hmim][Tf_2N] is expected to be larger than in the bulk IL. These computational findings are consistent with the recent experimental work by Baltus and colleagues showing that CO_2 permeability in an alumina confined IL is larger than in the bulk IL.[8] In the case of water, due to strong water hydrogen-bonding interactions with [hmim][Tf_2N], water molecules are not absorbed close to the silica walls, and water self-diffusivity is correlated to IL dynamics. At 298 K water self-diffusivity in the confined IL was found to be 1.8 times larger than in the bulk IL partly due to the faster dynamics

of the confined IL at 298 K. At 373 K, water self-diffusivity in the confined and bulk ILs are comparable.

An atomistic silica potential model was also used to calculate gas and IL self-diffusivity. The CO_2 self-diffusivity coefficients in the confined IL obtained from the atomistic and smooth silica potential models are similar. Although the atomistic silica potential model gives density distributions for the confined IL similar to the smooth silica model, it gives much larger self-diffusivity at 313 K and slightly larger self-diffusivity at 373 K than the smooth silica model. Similar to the smooth silica potential model, the atomistic silica model predicts much larger CO_2 self-diffusivity in the confined IL than in the bulk IL; the confined IL exhibits larger self-diffusivity at lower temperatures but smaller self-diffusivity at higher temperatures than the bulk IL. Furthermore, when the solid-fluid interaction is increased by a factor of eight, CO_2 self-diffusivity in the confined IL is still 5.8 times larger than in the bulk IL even though the confined IL itself exhibits 7.5 times smaller self-diffusivity than the bulk IL.

5 Acknowledgments

This technical effort was performed in support of the National Energy Technology Laboratory's on-going research in computational chemistry under the RES contract DE-FE0004000. We would also like to thank R. R. Anderson for his help in preparing this manuscript.

Supporting Information Available

Details for the acceptance rule of area A change in $NP_{xy}T$ Monte Carlo simulations, to build the atomistic silica slit pores, validation of the FGSF method against the standard Ewald method to compute electrostatic interactions in 2-D silica slit pores, and CO_2, N_2, H_2, and H_2O gases adsorption in empty silica slit pores are available in the supporting information. This material is available free of charge via the Internet at `http://pubs.acs.org`.

References

(1) Welton, T. Room-temperature ionic liquids. Solvents for synthesis and catalysis. *Chem. Rev.* **1999**, *99*, 2071–2083.

(2) Brennecke, J. F.; Maginn, E. J. Ionic liquids: Innovative fluids for chemical processing. *AIChE J.* **2001**, *47*, 2384–2389.

(3) Anderson, J.; Armstrong, D. High-stability ionic liquids. A new class of stationary phases for gas chromatography. *Anal. Chem.* **2003**, *75*, 4851–4858.

(4) Shi, W.; Sorescu, D. C. Molecular simulations of CO_2 and H_2 sorption into ionic liquid 1-n-Hexyl-3-methylimidazolium Bis(trifluoromethylsulfonyl)amide ([hmim][Tf_2N]) confined in carbon nanotubes. *J. Phys. Chem. B* **2010**, *114*, 15029–15041.

(5) Singh, R.; Monk, J.; Hung, F. R. Heterogeneity in the Dynamics of the Ionic Liquid [BMIM][PF_6] Confined in a Slit Nanopore. *J. Phys. Chem. C* **2011**, *115*, 16544–16554.

(6) Rajput, N. N.; Monk, J.; Singh, R.; Hung, F. R. On the Influence of Pore Size and Pore Loading on Structural and Dynamical Heterogeneities of an Ionic Liquid Confined in a Slit Nanopore. *J. Phys. Chem. C* **2012**, *116*, 5170–5182.

(7) Iacob, C.; Sangoro, J. R.; Kipnusu, W. K.; Valiullin, R.; Kaerger, J.; Kremer, F. Enhanced charge transport in nano-confined ionic liquids. *Soft Matter* **2012**, *8*, 289–293.

(8) Close, J. J.; Farmer, K.; Moganty, S. S.; Baltus, R. E. CO_2/N_2 separations using nanoporous alumina-supported ionic liquid membranes: Effect of the support on separation performance. *J. Membr. Sci.* **2012**, *390*, 201–210.

(9) Coasne, B.; Hung, F.; Pellenq, R.; Siperstein, F.; Gubbins, K. Adsorption of sample gases in MCM-41 materials: The role of surface roughness. *Langmuir* **2006**, *22*, 194–202.

(10) Schoen, M.; Diestler, D.; Cushman, J. Fluids in Micropores .4. The behavior of Molecularly thin confined films in the grand isostress ensemble. *J. Chem. Phys.* **1994**, *100*, 7707–7717.

(11) Spyriouni, T.; Economou, I. G.; Theodorou, D. N. Phase equilibria of mixtures containing chain molecules predicted through a novel simulation scheme. *Phys. Rev. Lett.* **1998**, *80*, 4466–4469.

(12) Shi, W.; Maginn, E. J. Continuous fractional component Monte Carlo: An adaptive biasing method for open system atomistic simulations. *J. Chem. Theory Comput.* **2007**, *3*, 1451–1463.

(13) Moucka, F.; Lísal, M.; Skvor, J.; Jirsak, J.; Nezbeda, I.; Smith, W. R. Molecular simulation of aqueous electrolyte solubility. 2. Osmotic ensemble Monte Carlo methodology for free energy and solubility calculations and application to NaCl. *J. Phys. Chem. B* **2011**, *115*, 7849–7861.

(14) Shi, W.; Maginn, E. J. Improvement in molecule exchange efficiency in Gibbs ensemble Monte Carlo: Development and implementation of the continuous fractional component move. *J. Comput. Chem.* **2008**, *29*, 2520–2530.

(15) Shi, W.; Maginn, E. J. Atomistic simulation of the absorption of carbon dioxide and water in the ionic liquid 1-n-hexyl-3-methylimidazolium bis(trifluoromethylsulfonyl)imide ([hmim][Tf_2N]). *J. Phys. Chem. B* **2008**, *112*, 2045–2055.

(16) Allen, M. P.; Tildesley, D. J. *Computer Simulation of Liquids*; Clarendon: Oxford, 1987.

(17) Travis, K.; Gubbins, K. Transport diffusion of oxygen-nitrogen mixtures in graphite pores: A nonequilibrium molecular dynamics (NEMD) study. *Langmuir* **1999**, *15*, 6050–6059.

(18) Steele, W. A. Physical interaction of gases with crystalline solids .1. Gas-solid energies and properties of isolated adsorbed atoms. *Surf. Sci.* **1973**, *36*, 317–352.

(19) Pinilla, C.; Del Popolo, M.; Lynden-Bell, R.; Kohanoff, J. Structure and dynamics of a confined ionic liquid. topics of relevance to dye-sensitized solar cells. *J. Phys. Chem. B* **2005**, *109*, 17922–17927.

(20) Phillips, J. C.; Braun, R.; Wang, W.; Gumbart, J.; Tajkhorshid, E.; Villa, E.; Chipot, C.; Skeel, R. D.; Kale, L.; Schulten, K. Scalable molecular dynamics with NAMD. *J. Comput. Chem.* **2005**, *26*, 1781–1802.

(21) Beutler, T. C.; Mark, A. E.; van Schaik, R. C.; Gerber, P. R.; van Gunsteren, W. F. Avoiding singularities and numerical instabilities in free-energy calculations based on molecular simulations. *Chem. Phys. Lett.* **1994**, *222*, 529–539.

(22) Shi, W.; Maginn, E. J. Molecular simulation and regular solution theory modeling of pure and mixed gas absorption in the ionic liquid 1-n-hexyl-3-methylimidazolium bis(trifluoromethylsulfonyl)imide ([hmim][Tf_2N]). *J. Phys. Chem. B* **2008**, *112*, 16710–16720.

(23) Shi, W.; Sorescu, D. C.; Luebke, D. R.; Keller, M. J.; Wickramanayake, S. Molecular simulations and experimental studies of solubility and diffusivity for pure and mixed gases of H_2, CO_2, and Ar absorbed in the ionic liquid 1-n-Hexyl-3-methylimidazolium Bis(Trifluoromethylsulfonyl)amide ([hmim][Tf_2N]). *J. Phys. Chem. B* **2010**, *114*, 6531–6541.

(24) Widegren, J.; Magee, J. Density, viscosity, speed of sound, and electrolytic conductivity for the ionic liquid 1-Hexyl-3-methylimidazolium Bis(trifluoromethylsulfonyl)imide and its mixtures with water. *J. Chem. Eng. Data* **2007**, *52*, 2331–2338.

(25) Kandil, M. E.; Marsh, K. N.; Goodwin, A. R. H. Measurement of the viscosity, density, and electrical conductivity of 1-Hexyl-3-methylimidazolium Bis(trifluorosulfonyl)imide at temperatures between (288 and 433) K and pressures below 50 Mpa. *J. Chem. Eng. Data* **2007**, *52*, 2382–2387.

(26) Fennell, C. J.; Gezelter, J. D. Is the Ewald summation still necessary? Pairwise alternatives to the accepted standard for long-range electrostatics. *J. Chem. Phys.* **2006**, *124*, 234104.

(27) Mehlig, B.; Heermann, D. W.; Forrest, B. M. Hybrid Monte-Carlo method for condensed-matter systems. *Phys. Rev. B* **1992**, *45*, 679–685.

(28) Wang, F.; Landau, D. P. Efficient, Multiple-range random walk algorithm to calculate the density of states. *Phys. Rev. Lett.* **2001**, *86*, 2050–2053.

(29) Cadena, C.; Zhao, Q.; Snurr, R. Q.; Maginn, E. J. Molecular modeling and experimental studies of the thermodynamic and transport properties of pyridinium-based ionic liquids. *J. Phys. Chem. B* **2006**, *110*, 2821–2832.

(30) Carman, P.; Stein, L. Self-diffusion in mixtures Part 1. Theory and its application to a nearly ideal binary liquid mixture. *Trans. Faraday Soc.* **1956**, *52*, 619–627.

(31) Krishna, R.; van Baten, J. The darken relation for multicomponent diffusion in liquid mixtures of linear alkanes: An investigation using molecular dynamics (MD) simulations *Ind. Eng. Chem. Res.* **2005**, *44*, 6939–6947.

(32) Gelb, L. D.; Gubbins, K. E. Phase separation in confined systems. *Rep. Prog. Phys.* **1999**, *62*, 1573–1569.

(33) Goebel, R.; Hesemann, P.; Weber, J.; Moeller, E.; Friedrich, A.; Beuermann, S.; Taubert, A. Surprisingly high, bulk liquid-like mobility of silica-confined ionic liquids. *Phys. Chem. Chem. Phys.* **2009**, *11*, 3653–3662.

(34) Singh, M. P.; Singh, R. K.; Chandra, S. Properties of ionic liquid confined in porous silica matrix. *ChemPhysChem* **2010**, *11*, 2036–2043.

(35) Singh, M. P.; Singh, R. K.; Chandra, S. Studies on imidazolium-based ionic liquids having a large anion confined in a nanoporous silica gel matrix. *J. Phys. Chem. B* **2011**, *115*, 7505–7514.

(36) Chen, S.; Wu, G.; Sha, M.; Huang, S. Transition of ionic liquid [bmim][PF_6] from liquid

to high-melting-point crystal when confined in multiwalled carbon nanotubes. *J. Am. Chem. Soc.* **2007**, *129*, 2416–2417.

(37) Shi, W.; Damodaran, K.; Nulwala, H. B.; Luebke, D. R. Theoretical and experimental studies of water interaction in acetate based ionic liquids. *Phys. Chem. Chem. Phys.* **2012**, *14*, 15897–15908.

(38) Zhang, J.; Zhang, Q.; Li, X.; Liu, S.; Ma, Y.; Shi, F.; Deng, Y. Nanocomposites of ionic liquids confined in mesoporous silica gels: preparation, characterization and performance. *Phys. Chem. Chem. Phys.* **2010**, *12*, 1971–1981.

(39) Cruz-Chu, E. R.; Aksimentiev, A.; Schulten, K. Water-silica force field for simulating nanodevices. *J. Phys. Chem. B* **2006**, *110*, 21497–21508.

Table 1: **Molar volume V_m for the confined [hmim][Tf_2N] in silica pores (25-45 Å) obtained from NP$_{xy}$T Monte Carlo simulations at 313-573 K and a pressure tensor P_{xy} of l bar. Also shown are the computed averages for simulation box lengths of L_x and L_y in the xy-plane. The uncertainty in the last digit is given in parentheses.**

pore width (Å)	T (K)	V_m (cm^3/mol)	$L_x = L_y$ (Å)
25	313	414.9 (5)	40.66 (3)
25	423	444 (1)	42.07 (6)
25	573	534 (5)	46.1 (2)
35	313	375.0 (9)	32.67 (4)
35	423	410 (1)	34.17 (4)
35	573	497 (2)	37.61 (8)
45	313	369 (1)	28.61 (4)
45	423	397.9 (7)	29.68 (2)
45	573	473 (1)	32.36 (4)

Table 2: **Self-diffusivity (D) coefficients in the xy-plane for CO_2, H_2, N_2, and H_2O gases absorption in [hmim][Tf_2N] confined in a 25 Å -silica slit pore. The results were obtained from NVE molecular dynamics simulations using the smooth silica potential model. The system consists of five gas molecules and 60 pairs of confined cations and anions. The gas self-diffusivities in the bulk ionic liquid (IL) at 3 mol% are also shown for comparison. All self-diffusivities were calculated in this work except that self-diffusivity coefficients for CO_2 and H_2 in the bulk IL were obtained from the previous work.[23] The values of $\beta = d(log\Delta r^2)/d(logt)$ are also shown. Uncertainties from simulations in the last digit are given in parentheses.**

		in confined IL		in bulk IL	
gas	T (K)	D (m^2/s)	β	D (m^2/s)	β
CO_2	313	$2.16(5)\times10^{-9}$	1.05(2)	$2.59(4)\times10^{-10}$	1.00(1)
CO_2	373	$3.06(2)\times10^{-9}$	0.95(1)	$1.26(1)\times10^{-9}$	0.99(1)
CO_2	573	$2.78(6)\times10^{-8}$	1.03(2)	$8.4(4)\times10^{-9}$	0.98(5)
H_2	313	$1.21(4)\times10^{-8}$	0.79(2)	$3.15(6)\times10^{-9}$	0.98(2)
H_2	373	$3.07(2)\times10^{-8}$	1.00(1)	$8.3(2)\times10^{-9}$	1.01(2)
H_2	573	$1.82(3)\times10^{-7}$	1.03(2)	$4.03(6)\times10^{-8}$	1.00(1)
N_2	298	$1.39(5)\times10^{-9}$	1.02(4)	$2.6(1)\times10^{-10}$	0.97(5)
N_2	373	$5.8(2)\times10^{-9}$	0.97(3)	$1.69(2)\times10^{-9}$	1.02(1)
H_2O	298	$1.49(5)\times10^{-10}$	1.00(4)	$8.5(2)\times10^{-11}$	1.03(2)
H_2O	373	$8.5(1)\times10^{-10}$	0.94(1)	$8.5(2)\times10^{-10}$	1.00(2)

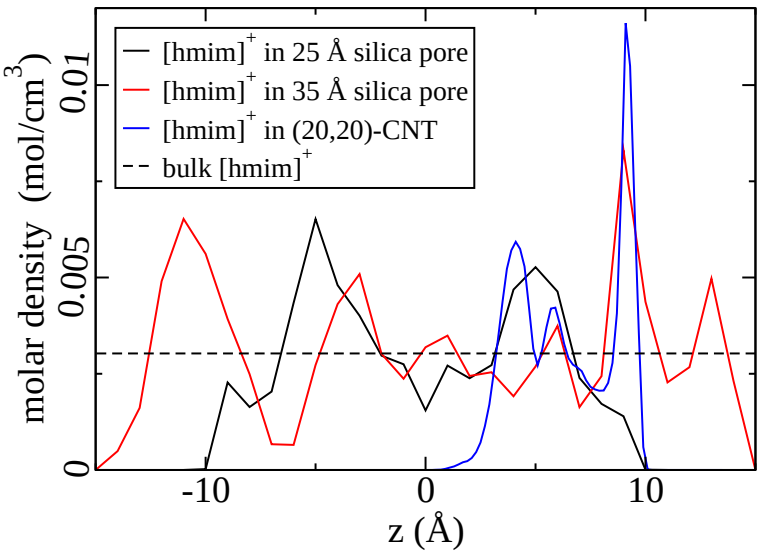

Figure 1: Local molar density of the center of mass for $[hmim]^+$ cations in silica slit pores. The results were obtained from $NP_{xy}T$ Mote Carlo simulations at 313 K and $P_{xy} = 1$ bar. For comparison, the cation densities in the bulk[23] and confined [hmim][Tf_2N] in a (20,20)-carbon nanotube (CNT)[4] at 313 K and 1 bar are also shown. The legends are as follows: black solid and red solid lines for the 25 Å- and 35 Å-silica slit pores, respectively; blue solid line for the (20,20)-CNT; and black dashed line for the bulk ionic liquid. Note that running longer simulations will lead to more smooth and symmetric density distributions. In the case of CNT, the z axis represents the radial distance of the C atom away from the CNT tube center. This radial distance is greater than zero and hence there is only 1/2 of the profile for the CNT.

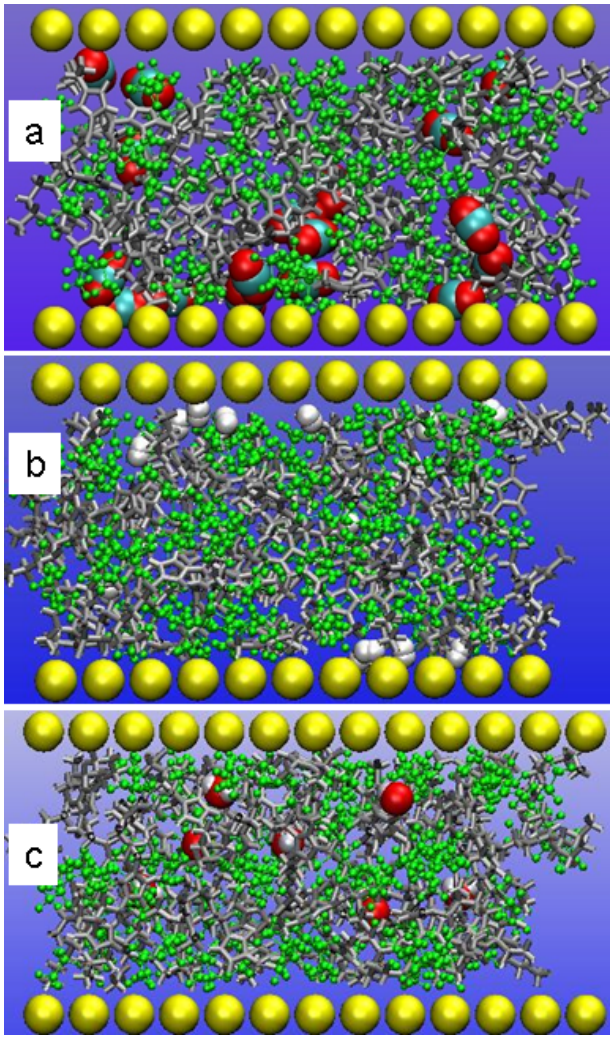

Figure 2: Snapshots for CO_2, H_2, and H_2O gaseous absorption in [hmim][Tf_2N] confined in a 25 Å-silica slit pore. Isostress-osmotic Monte Carlo simulations were implemented using the smooth silica potential model. The gas molecules are indicated using the vdw graphical representation. The colors for gas molecules are: red for oxygen atoms of CO_2 and H_2O, cyan for carbon atom of CO_2, and white for hydrogen atoms of H_2 and H_2O. The $[hmim]^+$ cations (gray) and $[Tf_2N]^-$ anions (green) are shown using the Bonds graphical representation. The silica walls are schematically represented by yellow spheres. Panel (a) indicates CO_2 absorption at 333 K and 8 bar; the corresponding average L_x and L_y values in the xy plane are 40.95 Å. Panel (b) corresponds to H_2 absorption at 313 K and 100 bar; the L_x and L_y values are 40.28 Å. Panel (c) is for H_2O absorption at 373 K and 0.2 bar; the L_x and L_y values are 41.01 Å.

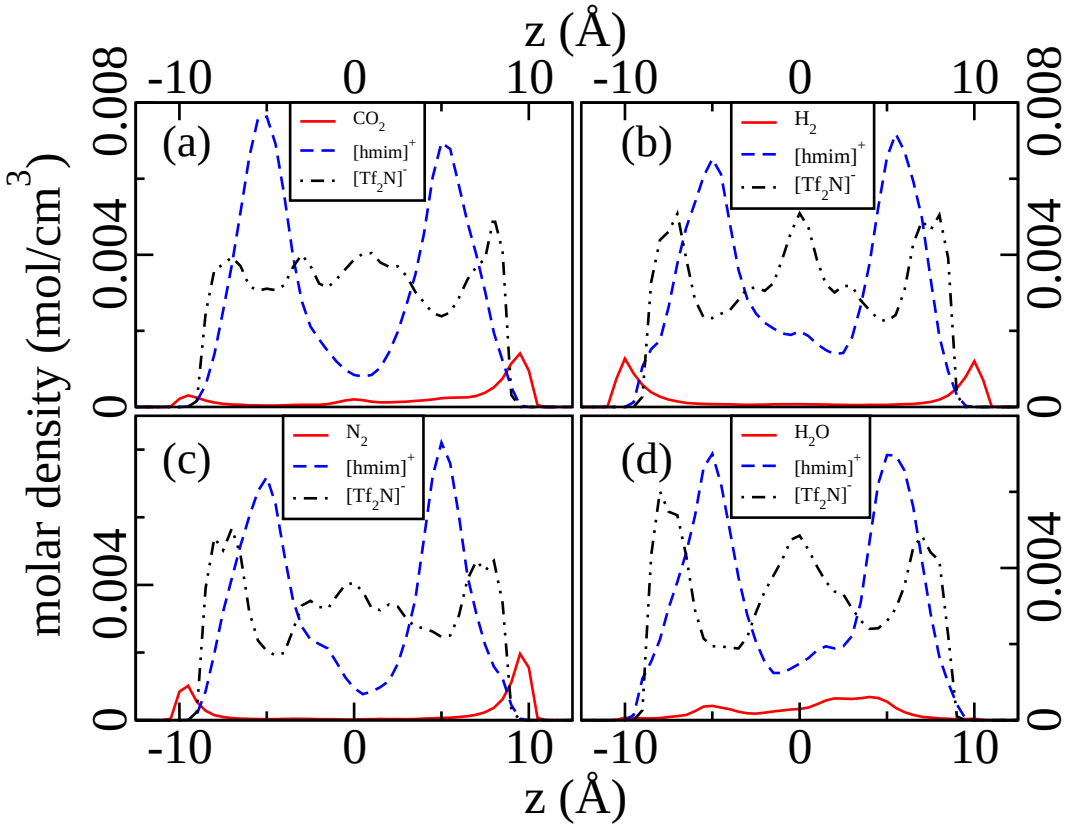

Figure 3: Molar density distributions for the center of mass of CO_2, H_2, N_2, H_2O gases, $[hmim]^+$ cations, and $[Tf_2N]^-$ anions confined in a 25 Å-silica slit pore. The results were obtained from molecular dynamics simulations using the smooth silica potential model. The panels are: (a) for CO_2 absorption at 313 K; (b) for H_2 absorption at 313 K; (c) for N_2 absorption at 298 K; and (d) for H_2O absorption at 298 K. Each system consists of five gas molecules and 60 pairs of cations and anions. The solid line indicates the density distribution for the gas; the dashed and dot-dashed lines are for the $[hmim]^+$ cation and $[Tf_2N]^-$ anion, respectively.

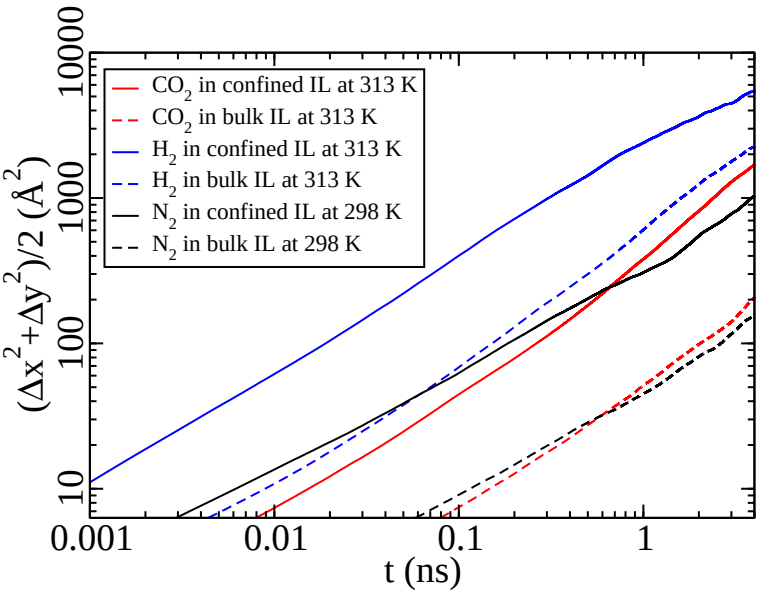

Figure 4: Mean squared displacement (MSD) in the *xy*-plane for the center of mass of CO_2, H_2, and N_2 gases in silica-pore confined [hmim][Tf_2N] (solid lines). The MSD values were obtained from NVE molecular dynamics simulations using the smooth silica potential model for systems consisting of five gas and 60 ionic liquid (IL) molecules confined in a 25Å-silica slit pore. For comparison, MSD values for corresponding gas absorption in the bulk IL are also shown at low gas concentrations of 3 mol% (dashed lines). The legends are as follows: red solid and red dashed lines for CO_2 at 313 K; blue solid and blue dashed lines for H_2 at 313 K; and black solid and black dashed lines for N_2 at 298 K.

Supporting Information

Enhanced Gas Absorption in the Ionic Liquid 1-n-Hexyl-3-methylimidazolium Bis(Trifluoromethylsulfonyl)amide ([hmim][Tf_2N]) Confined in Silica Slit Pores: A Molecular Simulation Study

Wei Shi,[*,†,‡,¶] and David R. Luebke[†]

U. S. Department of Energy, National Energy Technology Laboratory, Pittsburgh, PA 15236, USA, URS Corporation, South Park, PA 15129, USA, and Department of Chemical and Petroleum Engineering, University of Pittsburgh, Pittsburgh, PA 15261, USA

E-mail: shiw@netl.doe.gov

Acceptance rule for the area A change in $NP_{xy}T$ Monte Carlo simulations

In the $NP_{xy}T$ ensemble, the area A was changed using the following procedure,

[*]To whom correspondence should be addressed
[†]U. S. Department of Energy, National Energy Technology Laboratory, Pittsburgh, PA 15236, USA
[‡]URS Corporation, South Park, PA 15129, USA
[¶]Department of Chemical and Petroleum Engineering, University of Pittsburgh, Pittsburgh, PA 15261, USA

1. $A_{\text{new}} = A_{\text{old}} + \Delta A_{\max} \times (2.0 \times \xi - 1)$, where $\Delta A_{\max}$ is the maximum change in A, ξ is a random number between 0 and 1, A_{new} and A_{old} are the wall areas in the xy-plane after and before A is changed, respectively.

2. The x and y coordinates for the first atom of each molecule was scaled to new values by $x, y_{1,\text{new}} = x, y_{1,\text{old}} \times \frac{\sqrt{A_{\text{new}}}}{\sqrt{A_{\text{old}}}}$, where $x, y_{1,\text{old}}$ and $x, y_{1,\text{new}}$ are the x and y coordinates for the first atom of each molecule before and after the area change. All other atoms of each molecule are shifted in the xy-plane relative to the first atom according to $x, y_{i,\text{new}} = x, y_{i,\text{old}} + x, y_{1,\text{new}} - x, y_{1,\text{old}}$ for $i \geq 2$. Note that the box sizes in the x and y directions were set to be equal during simulations, i.e., $L_x = L_y = \sqrt{A}$.

3. The area change in step 1 was accepted or rejected using the following acceptance rule satisfying the detailed balance.

$$\frac{acc(o \to n)}{acc(n \to o)} = \exp\{-\beta[P_{xy}H(A_{\text{new}} - A_{\text{old}}) + (U_{\text{new}}^{\text{inter}} - U_{\text{old}}^{\text{inter}}) - Nk_BT \ln(\frac{A_{\text{new}}}{A_{\text{old}}})]\}, \qquad (1)$$

where β is the reduced temperature, k_B is the Boltzmann constant, $U_{\text{new}}^{\text{inter}}$ and $U_{\text{old}}^{\text{inter}}$ are the interaction energies after and respectively before the area change. Here, the interaction energy U^{inter} consists of the adsorbate-wall interaction and the interaction between the atoms of different adsorbate molecules as well as the interaction between the atoms in the same adsorbate molecule when these atoms are separated by at least three consecutive bonds. Examples of such intramolecular interactions considered here are the 1-4, 1-5, 1-6, etc. interactions. In Equation (1) the interaction energies are obtained as a summation over the total number of cation and anion species of the system, i.e., $N = N^+ + N^-$ for the ionic liquid (IL) molecules. Note that when the adsorbate-adsorbate interaction is small, the ideal gas law equation, i.e. $P_{xy}AH = Nk_BT$ can be roughly used. To test this idea gas behavior, a simulation was carried out for a simple Lennard-Jones (LJ) fluid confined in a silica slit pore. When the pressure tensor P_{xy} was set to be small, the interaction energy between the LJ particles was found to be small. This corresponds to a low adsorbate loading. Under these low P_{xy} conditions,

the ideal gas law equation was found to hold in simulations as expected. Additionally, the computed pressure tensor $P_{xy} = (P_{xx} + P_{yy})/2$ was found to be equal to the imposed P_{xy} value, which confirms that we have correctly implemented the pressure tensor calculations in our in-house code.

Validation of the Fennell and Gezelter shifted method in silica slit pores

The Fennell and Gezelter shifted (FGSF) force[1] method was evaluated against the standard Ewald technique to calculate the electrostatic interaction for IL molecules confined in silica slit pores. About 1000 configurations were collected from simulations using the 9-3 smooth potential (Equation (4) in the main text); each configuration consists of 60 [hmim][Tf_2N] molecules confined in a 25 Å-silica slit pore. The electrostatic energy was calculated for all the 1000 snap shots using both the Ewald and FGSF methods. Similar to the bulk IL[2] and IL confined in the CNT,[3] the electrostatic energy difference ΔE_{elec} for ILs confined in the silica slit pore between neighboring snap shots obtained from the FGSF method was found to be very close to the energy difference values obtained from the Ewald method. The difference in ΔE_{elec} between the Ewald and the FGSF methods is -0.13 kcal/mol to 0.10 kcal/mol per IL molecule, and the average difference was found to be very small, about 2.23×10^{-6} kcal/mol. Additionally, molar volume for confined IL obtained from the $NP_{xy}T$ Monte Carlo simulation using the FGSF method was found to be very close to the molar volume value using the Ewald method. For example, at 313 K and a pressure tensor P_{xy} of 1 bar, the IL molar volume difference between the FGSF and Ewald methods was found to be 0.8% and 0.6% for ILs confined in the 25 Å and 35Å-silica slit pores, respectively.

Adsorption isotherms of CO_2, H_2, N_2, and H_2O gas in empty silica slit pores

Pure CO_2, H_2, N_2, and H_2O gas adsorption in empty silica pores were conducted and the amounts of adsorption for CO_2 and H_2 in different silica pores are shown in Table S1. When the pore width

is increased, the amounts of CO_2 and H_2 adsorbed increase. The amounts of CO_2 adsorption at 333-573 K and 4-17 bar in a 25 Å-pore are about 1.4 and 1.7 times smaller than those in the 35 Å and 45 Å slit pores, respectively. The H_2 amounts of adsorption are 1.4 and 1.9 times smaller in a 25 Å-pore compared to the 35 Å and 45 Å pores, respectively. Interestingly, the amounts of gas adsorption is approximately proportional to the slit pore width. For example, when the slit pore width is increased from 25 Å to 35Å, the pore width is increased 1.4 times, which is very similar to the ratio value for the increased amounts of CO_2 and H_2 adsorption in a 25 Å -pore compared to a 35 Å -pore. This similarity is probably due to the weak fluid-silica interaction and consequently the pore volume is an important factor to determine gas adsorption.

Henry's Law constants for gas adsorption in silica pores were estimated from the linear fitting of fugacity versus number of gas adsorption per surface area in the *xy*-plane ($L_x \times L_y$ in Table S1). The Henry's Law constants for CO_2 and H_2 in silica slit pores (25 Å and 45 Å) at different temperatures are shown in Figure S1 (a) . The CO_2 amounts of adsorption are about two times larger than H_2 at 313-573 K. The corresponding Henry's Law constants for H_2O and N_2 at 298-373 K adsorbed in a 25 Å-silica slit pore are shown in Figure S1 (b). At 333-373 K, the gas adsorption decreases in the following order: $H_2O > CO_2 > N_2 > H_2$. As shown in Figure S1 (a) and (b), the amounts of CO_2, H_2, N_2, and H_2O adsorption in silica slit pores decreases when the temperature is increased. The adsorption enthalpy was also found to be small. For example, the CO_2 adsorption enthalpy values were estimated to be -5.1 ± 0.1 kJ/mol and 4.6 ± 0.1 kJ/mol in the 25Å and 45 Å slit pores, respectively. For H_2, the adsorption enthalpy values were computed to be about -3.4 ± 0.2 kJ/mol.

Construction of the atomistic silica slit pores

In order to study the effects of the atomistic details for the silica wall on the self-diffusivity values for gas absorbed in the confined ionic liquid, atomistic silica pores were constructed. A unit cell with dimensions $a = b = 4.599$ Å, $c = 6.130$ Å, and $\alpha = \beta = \gamma = 90$ ° for a high-pressure

polymorphism of silica cristobalite was chosen.[4] The space group is $P4_12_12$ and the crystal density is 3.078 g/cm^3. A large super cell was built using the Materials Studio 4.0 (Accelrys, San Diego, CA). A typical slab wall with dimensions of 45.99 Å $\times$45.99 Å $\times$7.66 Å was constructed by truncating the super cell; each slab wall consists of 490 Si atoms and 980 O atoms. By placing two such slabs opposite to each other separated by a distance of certain value (pore width), an atomistic silica slit pore was constructed. To minimize the interactions between adsorbate molecules in the primary cell and image cells in the z direction, the simulation box size in the z direction was set to be 124.04 Å with dimensions of 45.99 Å $\times$45.99 Å $\times$124.04 Å.

References

(1) Fennell, C. J.; Gezelter, J. D. Is the Ewald summation still necessary? Pairwise alternatives to the accepted standard for long-range electrostatics. *J. Chem. Phys.* **2006**, *124*, 234104.

(2) Shi, W.; Maginn, E. J. Atomistic Simulation of the Absorption of Carbon Dioxide and Water in the Ionic Liquid 1-n-hexyl-3-methylimidazolium bis(trifluoromethylsulfonyl) imide ([hmim][Tf_2N]). *J. Phys. Chem. B* **2008**, *112*, 2045–2055.

(3) Shi, W.; Sorescu, D. C. Molecular Simulations of CO_2 and H_2 Sorption into Ionic Liquid 1-n-Hexyl-3- methylimidazolium Bis(trifluoromethylsulfonyl)amide ([hmim][Tf_2N]) Confined in Carbon Nanotubes. *J. Phys. Chem. B* **2010**, *114*, 15029–15041.

(4) Dera, P.; Lazarz, J. D.; Prakapenka, V. B.; Barkley, M.; Downs, R. T. New insights into the high-pressure polymorphism of SiO_2 cristobalite. *Phys. Chem. Miner.* **2011**, *38*, 517–529.

Table S1: Calculated average number <*N*> of CO_2 and H_2 molecules adsorbed in silica slit pores obtained from continuous fractional component grand canonical Monte Carlo simulations. Also shown are the gas fugacity and the simulation box sizes of L_x and L_y. Fugacities for CO_2 and H_2 were computed from the Peng-Robinson equation of state[2] and molecular dynamics simulations, respectively. The uncertainty in the last digit is given in parentheses.

gas	temperature (K)	pressure (bar)	fugacity (bar)	pore width (Å)	$L_x = L_y$ (Å)	<*N*>
CO_2	333	4	3.9384	25	200	90.5 (2)
CO_2	333	8	7.7552	25	100	45.69 (8)
CO_2	333	17.15	16.04	25	60	35.80 (9)
CO_2	423	8	7.8936	25	100	33.24 (6)
CO_2	423	17.15	16.66637	25	60	25.67 (5)
CO_2	573	8	7.976	25	200	92.4 (2)
CO_2	573	17.15	17.04024	25	100	49.35 (7)
CO_2	333	4	3.9384	35	200	124.0 (1)
CO_2	333	8	7.7552	35	100	62.3 (1)
CO_2	333	17.15	16.04	35	60	48.86 (9)
CO_2	333	4	3.9384	45	200	156.1 (3)
CO_2	333	8	7.7552	45	100	79.0 (2)
CO_2	333	17.15	16.04	45	60	61.7 (1)
CO_2	423	8	7.8936	45	100	59.4 (1)
CO_2	423	17.15	16.66637	45	60	45.99 (5)
CO_2	573	8	7.976	45	200	170.6 (3)
CO_2	573	17.15	17.04024	45	100	91.1 (1)
H_2	313	50	51.3	25	40	41.1 (1)
H_2	313	100	105.3	25	40	79.9 (1)
H_2	373	50	51.2	25	40	34.2 (1)
H_2	373	100	104.8	25	40	66.6 (1)
H_2	573	50	50.6	25	40	21.90 (3)
H_2	573	100	102.8	25	40	43.1 (1)
H_2	313	50	51.3	35	40	59.0 (1)
H_2	313	100	105.3	35	40	114.8 (2)
H_2	313	50	51.3	45	40	77.1 (2)
H_2	313	100	105.3	45	40	150.3 (2)
H_2	373	50	51.2	45	40	64.7 (1)
H_2	373	100	104.8	45	40	126.1 (2)
H_2	573	50	50.6	45	40	41.8 (1)
H_2	573	100	102.8	45	40	82.1 (1)

Table S2: The average number ($\langle N \rangle$) of CO_2, H_2, N_2, and H_2O molecules absorbed in 60 [hmim][Tf_2N] cation/anion pairs confined in silica slit pores. The results were obtained from the continuous fractional component isostress-osmotic Monte Carlo simulation at different temperature T, pressure tensor P_{xy}, and gas fugacity f. The gas fugacities for CO_2, N_2, and H_2O were obtained from the Peng-Robinson equation of state,[2] and from molecular dynamics simulation for H_2. Also shown are the simulated box lengths of L_x and L_y in the xy-plane, and gas mole fraction ($x = \frac{\langle N \rangle}{\langle N \rangle + 60}$). The uncertainty in the last digit is given in parentheses.

gas	T (K)	P_{xy} (bar)	f (bar)	pore width (Å)	$L_x = L_y$ (Å)	$\langle N \rangle$	x
CO_2	333	4	3.9384	25	40.76 (6)	7.0 (3)	0.104 (4)
CO_2	333	4	3.9384	35	33.01 (3)	5.8 (3)	0.087 (4)
CO_2	333	4	3.9384	45	28.82 (3)	4.5 (3)	0.069 (4)
CO_2	333	8	7.7552	25	40.95 (5)	15.0 (8)	0.198 (9)
CO_2	333	8	7.7552	35	33.22 (6)	11.9 (7)	0.164 (8)
CO_2	333	8	7.7552	45	29.12 (3)	10.5 (4)	0.148 (4)
CO_2	333	17.15	16.04	25	41.89 (5)	30.1 (8)	0.332 (6)
CO_2	333	17.15	16.04	35	33.72 (4)	24.3 (7)	0.287 (6)
CO_2	423	8	7.8936	25	42.05 (3)	4.2 (1)	0.065 (2)
CO_2	423	17.15	16.66637	25	42.89 (3)	11.2 (4)	0.156 (4)
CO_2	423	35	33.0295	25	42.59 (6)	18.7 (7)	0.238 (8)
CO_2	423	83.6	73.09148	25	44.1 (1)	48 (1)	0.440 (6)
CO_2	573	8	7.976	25	45.51 (6)	2.60 (7)	0.041 (1)
CO_2	573	17.15	17.04024	25	46.0 (2)	5.9 (2)	0.088 (3)
CO_2	573	35	34.5555	25	47.2 (1)	13.7 (4)	0.183 (4)
CO_2	573	83.6	81.29264	25	47.1 (2)	28.2 (8)	0.317 (6)
H_2	313	50	51.3	25	39.95 (6)	4.7 (2)	0.071 (2)
H_2	313	50	51.3	35	32.61 (2)	3.1 (1)	0.051 (1)
H_2	313	50	51.3	45	28.64 (3)	3.8 (1)	0.058 (2)
H_2	313	100	105.3	25	40.28 (4)	10.6 (2)	0.148 (2)
H_2	313	100	105.3	35	32.59 (2)	6.8 (2)	0.100 (3)
H_2	313	100	105.3	45	28.40 (2)	5.8 (2)	0.087 (2)
H_2	313	200	221.8	25	40.18 (3)	19.5 (3)	0.244 (3)
H_2	313	200	221.8	35	32.46 (3)	11.0 (4)	0.153 (5)
H_2	313	300	350.7	25	40.24 (5)	28.8 (6)	0.322 (5)
H_2	313	300	350.7	35	32.68 (3)	19.2 (5)	0.240 (4)
H_2	373	50	51.2	25	41.13 (6)	4.9 (1)	0.074 (2)
H_2	373	100	104.8	25	41.09 (5)	9.6 (2)	0.136 (3)
H_2	373	200	219.4	25	40.91 (4)	18.3 (4)	0.231 (4)
H_2	573	50	50.6	25	45.6 (1)	6.9 (2)	0.101 (2)
H_2	573	100	102.8	25	46.8 (1)	16.7 (4)	0.215 (4)
H_2	573	200	213.2	25	45.55 (9)	26.5 (4)	0.304 (3)
N_2	298	40	39.4	25	40.48 (4)	9.3 (3)	0.129 (4)
N_2	298	80	78.0240	25	40.88 (5)	19.3 (6)	0.241 (5)
N_2	298	120	116.4720	25	40.65 (4)	23.1 (4)	0.276 (3)
N_2	298	200	194.76	25	40.67 (4)	30.4 (7)	0.335 (5)
N_2	298	500	544.5	25	40.71 (7)	48 (1)	0.440 (7)
N_2	333	50	49.76	25	40.42 (6)	7.0 (3)	0.103 (4)
N_2	333	100	99.6	25	40.66 (4)	13.9 (3)	0.186 (4)
N_2	333	200	202.4	25	40.67 (6)	20.8 (7)	0.255 (6)
N_2	333	500	572.0	25	40.65 (3)	38.6 (7)	0.390 (4)
H_2O	373	0.05	0.05	25	41.13 (7)	1.7 (3)	0.027 (4)
H_2O	373	0.1	0.1	25	41.04 (9)	3.4 (4)	0.052 (6)
H_2O	373	0.2	0.2	25	41.01 (5)	7.2 (4)	0.105 (5)

Table S3: **Specific non-bonded energy U_{IL}^{nb}, U_{sf}^{nb}, U_{t}^{nb}, and bonded energy U_{IL}^{b} for [hmim][Tf_2N] confined in silica slit pores. The U_{IL}^{nb} energy consists of van der Waals and electrostatic interactions between IL molecules. The U_{sf}^{nb} indicates interaction between ionic liquid molecules and silica walls. The U_{t}^{nb} energy is the summation of U_{IL}^{nb} and U_{sf}^{nb}. All the interaction energies were obtained at 313 K and a pressure tensor P_{xy} of 1 bar. For comparison, the corresponding energies for the bulk and confined IL in a (20,20)-carbon nanotube (CNT) are also shown.[3] The Fennel and Gezelter shift force (FGSF)[1] method was used to calculate the electrostatic interaction energy. The specific energies were obtained from the corresponding extensive values divided by the number of ion pairs. The uncertainty in the last digit is given in parentheses.**

system	U_{t}^{nb} (kJ/mol)	U_{IL}^{nb} (kJ/mol)	U_{sf}^{nb} (kJ/mol)	U_{IL}^{b} (kJ/mol)
25 Å silica	−128.8 (3)	−120.6 (3)	−8.19 (3)	159.0 (1)
35 Å silica	−133.6 (3)	−127.5 (3)	−6.11 (4)	158.6 (1)
45 Å silica	−135.0 (3)	−130.8 (3)	−4.23 (4)	158.7 (1)
bulk IL	−140.5 (1)	−140.5 (1)	0	161.4 (1)
(20,20)-CNT	−171.6 (2)	−100.8 (2)	−70.8 (4)	159.0 (1)

Table S4: **The number of CO_2 molecules adsorbed in a silica slit pore using the atomistic silica potential model. The pore has a width of 25 Å and a size of 45.99 Å in both the x and y directions. The results were obtained from continuous fraction component grand canonical Monte Carlo simulations. The CO_2 fugacities were computed from the Peng-Robinson equation of state.[2] The amounts of CO_2 adsorption in the same silica pore using the smooth silica potential model are also shown for comparison.**

temperature(K)	pressure (bar)	fugacity (bar)	amounts (atomistic)	amounts (smooth)
333	8	7.7552	11.0 ± 0.2	9.66 ± 0.02
333	17.15	16.04	24.2 ± 0.2	21.03 ± 0.05
423	8	7.8936	7.7 ± 0.1	7.03 ± 0.01
423	17.15	16.66637	16.3 ± 0.1	15.08 ± 0.03

Table S5: **Self-diffusivity (D) in the xy-plane using the atomistic silica potential model. The system consists of five CO_2 and 76-155 [hmim][Tf_2N] molecules confined in silica slit pores. For comparison CO_2 self-diffusivities in the bulk IL are also shown. The $\beta = d(log\Delta r^2)/d(logt)$ values from simulations are also given. Uncertainties from simulations in the last digit are given in parentheses.**

T (K)	system	D_+ (m^2/s)	β_+	D_- (m^2/s)	β_-	D_{CO_2} (m^2/s)	β_{CO_2}
313	25 Å	4.6(1) $\times 10^{-11}$	0.97(2)	5.0(1)$\times 10^{-11}$	1.03(2)	1.94(2) $\times 10^{-9}$	1.00(1)
373	25 Å	5.8(2) $\times 10^{-11}$	0.75(3)	6.4(2)$\times 10^{-11}$	0.82(4)	3.20(4) $\times 10^{-9}$	0.96(1)
313	45 Å	5.1(2) $\times 10^{-11}$	1.10(3)	4.8(2)$\times 10^{-11}$	1.12(3)	1.11(3) $\times 10^{-9}$	1.00(3)
373	45 Å	2.04(2) $\times 10^{-10}$	0.98(1)	2.02(2)$\times 10^{-10}$	1.01(1)	2.23(3) $\times 10^{-9}$	0.95(1)
313	bulk IL	1.24(4) $\times 10^{-11}$	0.99(3)	8.7(4)$\times 10^{-12}$	0.96(4)	2.59(4) $\times 10^{-10}$	1.00(1)
373	bulk IL	8.3(1) $\times 10^{-11}$	1.03(1)	6.82(3)$\times 10^{-11}$	1.00(1)	1.26(1) $\times 10^{-9}$	0.99(1)

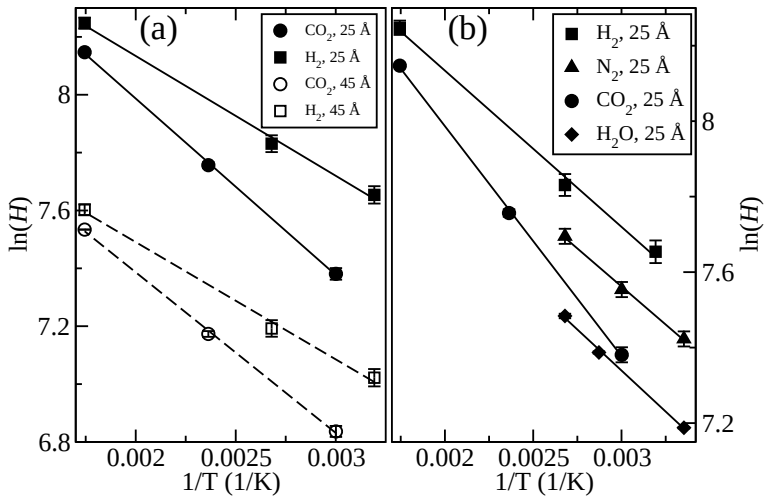

Figure S1: (a): A van't Hoff plot of the computed Henry's Law constants for CO_2 and H_2 adsorption in the 25 Å and 45 Å silica slit pores. The symbols are as follows: filled circles for CO_2 in the 25 Å silica slit pore; open circles for CO_2 in the 45 Å silica slit pore; filled squares for H_2 in the 25 Å silica slit pore; and open squares for H_2 in the 45 Å silica slit pore. (b): A van't Hoff plot of the computed Henry's Law constants for CO_2, H_2, N_2, and H_2O adsorption in a 25 Å -silica slit pore. The symbols are as follows: squares for H_2, triangles for N_2, circles for CO_2, and diamonds for H_2O. The lines are linear fitting to the simulated values.

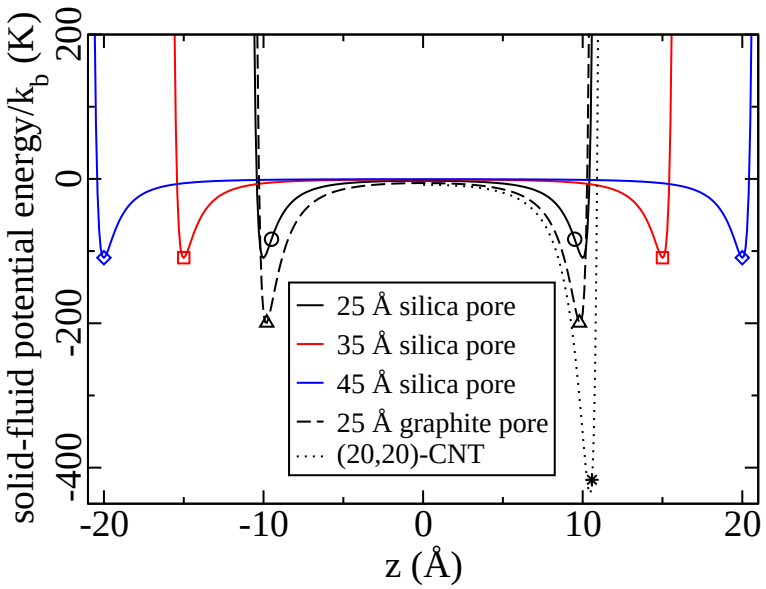

Figure S2: Solid-fluid interaction energy for the C atom of CO_2 molecule with silica walls as a function of the distance z between the C atom and silica wall. For comparison, the C atom interaction energies with a graphite slit pore and a (20,20)-carbon nanotube (CNT) are also shown. Solid lines with circle, square, and diamond symbols correspond to silica slit pores of width of 25 Å, 35 Å, and 45 Å, respectively. The dashed line with triangles is for the graphite slit pore (25 Å), and the dotted line with a star symbol indicates the (20,20)-CNT. Different symbols on lines are used for clarity. In the case of CNT, the z axis represents the radial distance of the C atom away from the CNT tube center. This radial distance is greater than zero and hence there is only 1/2 of the profile for the CNT.

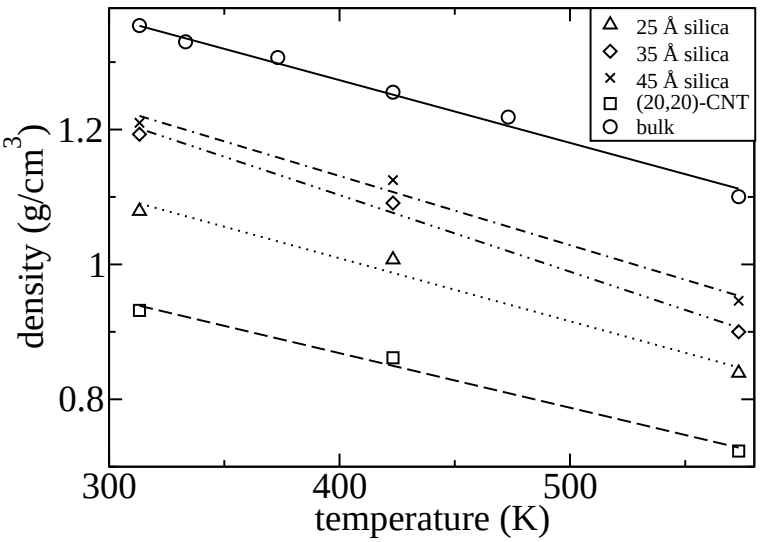

Figure S3: The density for confined [hmim][Tf_2N] in silica slit pores obtained from $NP_{xy}T$ Mote Carlo simulations at $P_{xy} = 1$ bar. The densities for the confined ionic liquid (IL) in a (20,20)-carbon nanotube (CNT)[3] and for the bulk IL at 1 bar are also shown for comparison. The triangle, diamond, and cross symbols are for silica slit pores of width of 25 Å, 35 Å, and 45 Å, respectively. The circles correspond to the bulk IL, and the squares indicate the results for the (20,20)-CNT. Each line represents the linear fitting of simulated values.

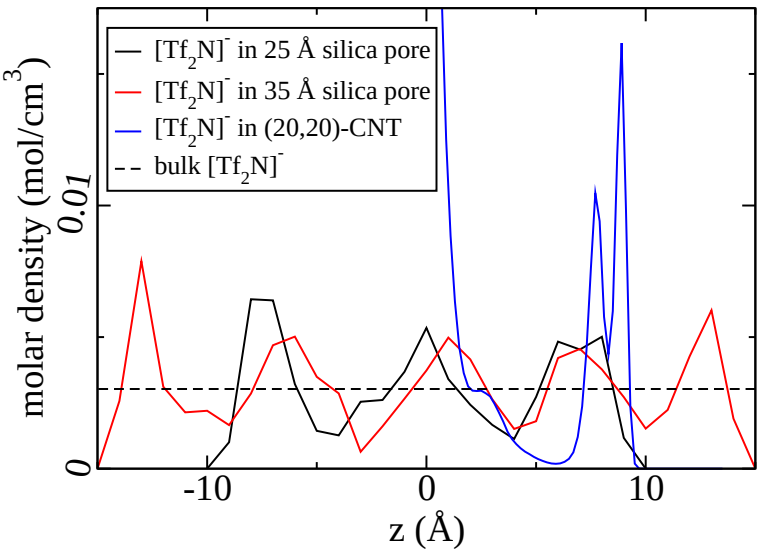

Figure S4: Local molar density of the center of mass for $[Tf_2N]^-$ anions in silica slit pores at 313 K and 1 bar. For comparison, the anion densities in the bulk and confined [hmim][Tf_2N] in a (20,20)-carbon nanotube (CNT)[3] at 313 K and 1 bar are also shown. The legends are as follows: black solid and red solid lines for the 25 Å- and 35 Å-silica slit pores, respectively; blue solid line for the (20,20)-CNT; and black dashed line for the bulk ionic liquid. Note that running longer simulations will lead to more smooth and symmetric density distributions. In the case of CNT, the z axis represents the radial distance of the C atom away from the CNT tube center. This radial distance is greater than zero and hence there is only 1/2 of the profile for the CNT.

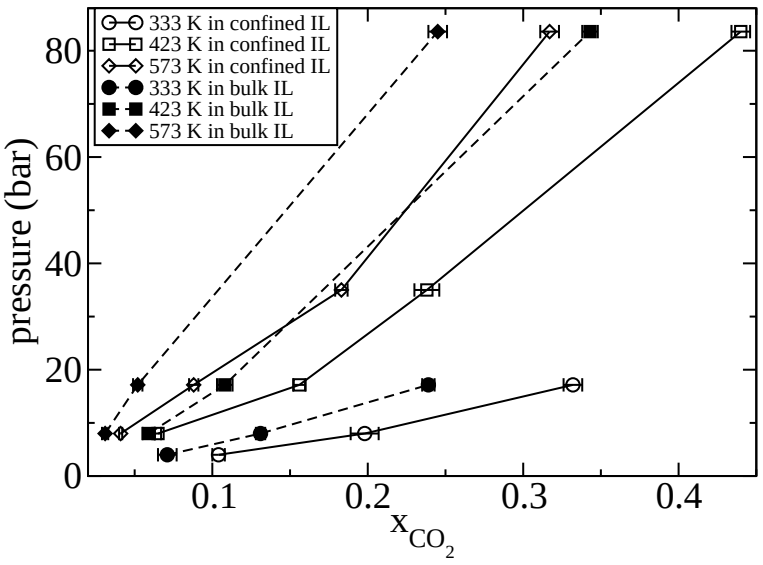

Figure S5: CO_2 absorption isotherms in silica-pore (25 Å) confined [hmim][Tf_2N] obtained from isostress-osmotic Monte Carlo simulations. For comparison, simulated CO_2 absorption isotherms in the bulk ionic liquid (IL)[2] are also shown. The legends are as follows: open circles, squares, and diamonds are for the confined IL at 333 K, 423 K, and 573 K, respectively; filled circles, squares, and diamonds are for the bulk IL at 333 K, 423 K, and 573 K, respectively. Error bars from simulations are also shown. The lines are guides to the eye.

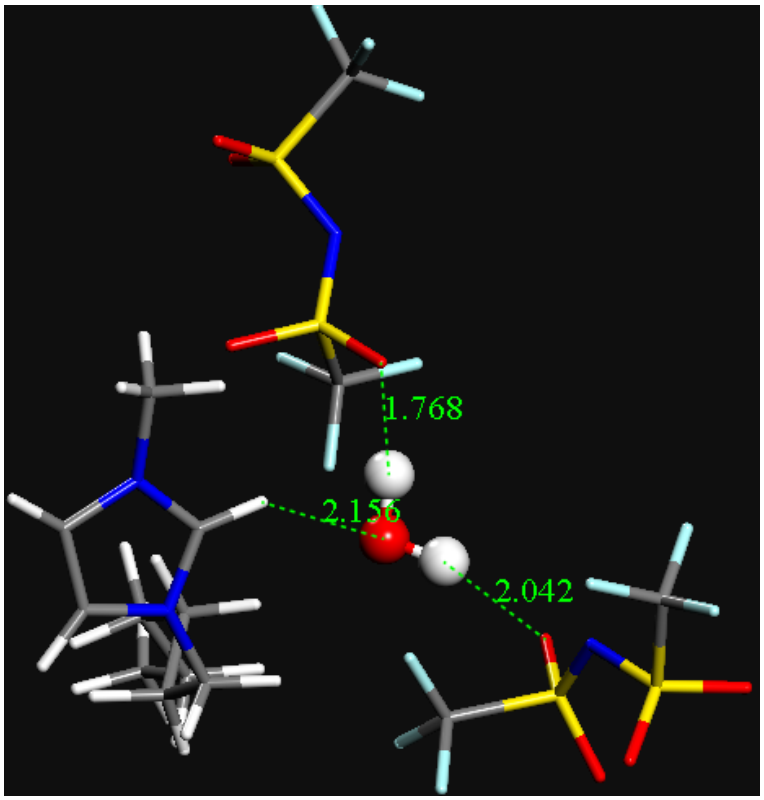

Figure S6: Snap shot from molecular dynamics simulations to show hydrogen-bonding interactions between one water molecule and the nearby $[hmim]^+$ cations and $[Tf_2N]^-$ anions confined in silica slit pores. The water molecule is indicated as the ball and stick representation. The ionic liquid molecules are shown using the stick representation. The atom pair distances for O/$[H_2O]$-H/$[hmim]^+$ and H/$[H_2O]$-O/$[Tf_2N]^-$ are also shown. The silica walls and all other water and ionic liquid molecules are not shown for clarity.

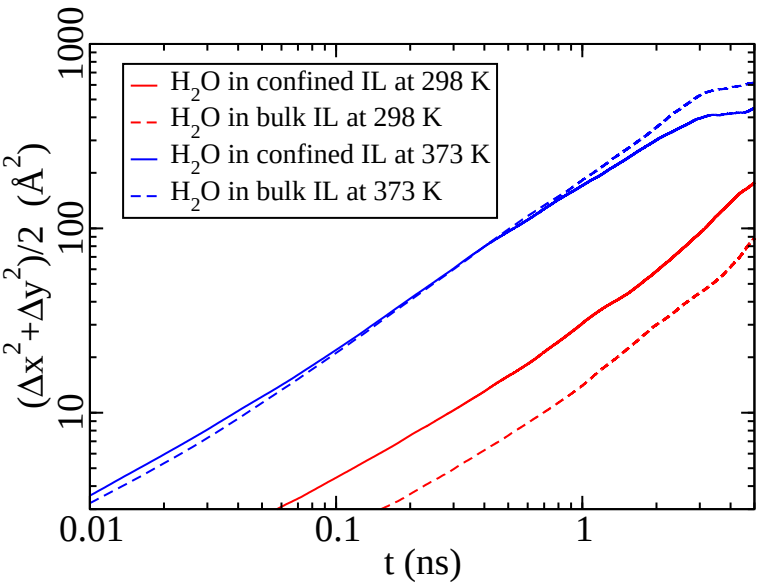

Figure S7: Mean squared displacement (MSD) in the *xy*-plane for the center of mass of H_2O absorption in silica-pore confined [hmim][Tf_2N]. The MSD values were obtained from NVE molecular dynamics simulations using the smooth silica potential model for a system consisting of five water and 60 ionic liquid (IL) molecules confined in a 25Å-silica slit pore. For comparison, MSD values for H_2O in the bulk IL are also shown at low water concentration of 3 mol%. The red solid and red dashed lines indicate MSD values of water at 298 K in the confined IL and bulk IL, respectively. The blue solid and blue dashed lines are for water at 373 K in the confined and bulk IL, respectively.

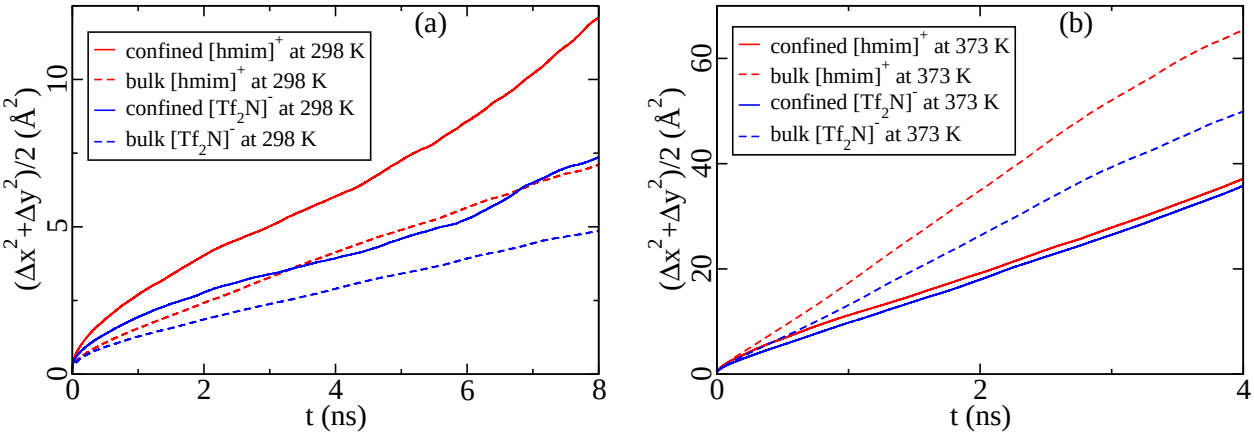

Figure S8: Mean squared displacement (MSD) in the *xy*-plane for the center of mass of $[hmim]^+$ cations and $[Tf_2N]^-$ anions confined in a 25Å-silica slit pore. The MSD values were obtained from NVE molecular dynamics simulations using the smooth silica potential model. For comparison, MSD values for the cations and anions in bulk [hmim][Tf_2N] are also shown. Panel (a) shows results at 298 K and the legends are as follows: red solid and red dashed lines are for $[hmim]^+$ cations in the confined and bulk ionic liquid (IL), respectively; blue solid and blue dashed lines are for $[Tf_2N]^-$ anions in the confined IL and bulk IL, respectively. Panel (b) shows results at 373 K and the legends are the same as those in Panel (a).

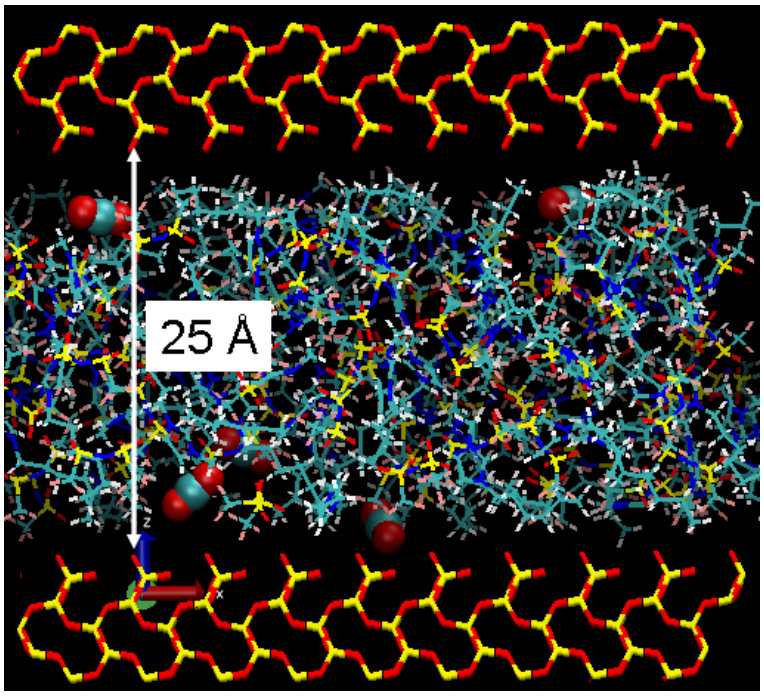

Figure S9: Snapshot from molecular dynamics simulations using the atomistic silica potential model. Simulations were performed at 313 K for five CO_2 and 76 [hmim][Tf_2N] molecules confined in a 25Å-silica slit pore. The two silica walls have a dimension of 45.99 Å $\times$ 45.99 Å $\times$ 7.66Å and consist of 980 Si and 1960 O atoms. The distance between two oxygen atoms on the opposite silica walls is also shown to roughly indicate the silica slit pore width. The CO_2 molecules are displayed using the vdw graphical representation, ionic liquid molecules are shown using the Lines graphical representation, and the atomistic silica structure is indicated by the Bonds representation.

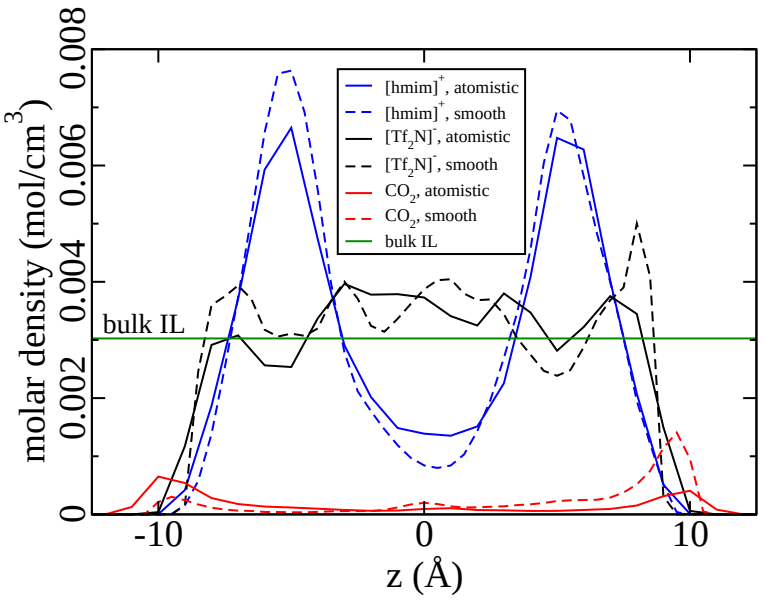

Figure S10: Molar density distributions for the center of mass of $[hmim]^+$ cations, $[Tf_2N]^-$ anions, and CO_2 molecules absorbed in an atomistic silica slit pore of width 25 Å (Figure S9). Simulations were performed at 313 K using an atomistic silica potential model. For comparison, the corresponding density distributions using the smooth silica potential model are also shown. The solid and dashed lines indicate the distributions using the atomistic and smooth silica potential models, respectively. The blue, black, and red lines are for $[hmim]^+$ cation, $[Tf_2N]^-$ anion, and CO_2, respectively. The horizontal green line corresponds to the simulated molar density for the $[hmim]^+$ cations and $[Tf_2N]^-$ anions in the bulk ionic liquid at 313 K.

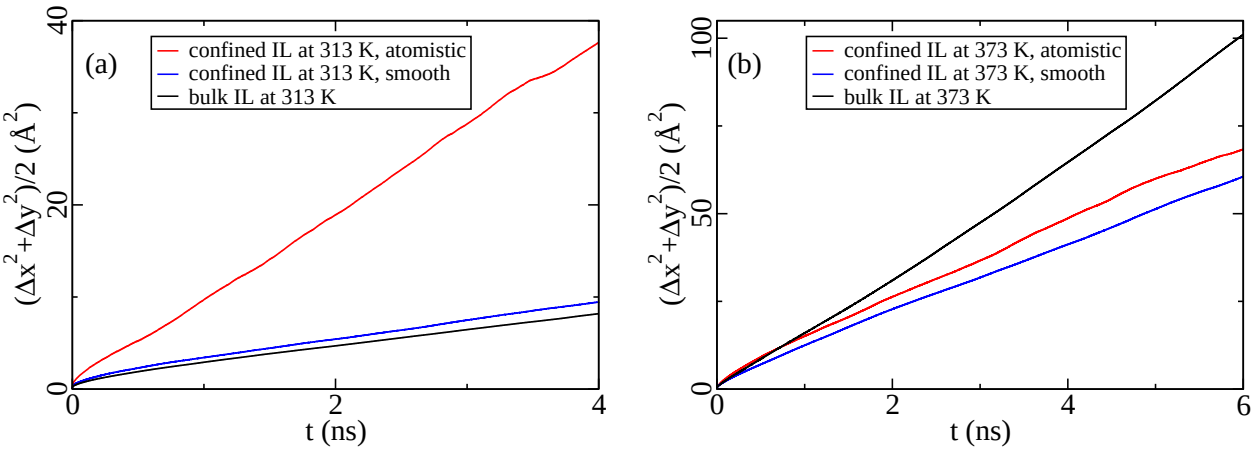

Figure S11: Mean squared displacement (MSD) in the *xy*-plane for the center of mass of [hmim][Tf_2N] confined in a 25 Å-silica slit pore (Figure S9) using an atomistic silica potential model. The MSD values for the ionic liquid (IL) were calculated as the arithmetic mean MSD values for the $[hmim]^+$ cation and $[Tf_2N]^-$ anion. The MSD values for confined IL in a 25 Å-silica pore using the smooth silica potential model, and for the bulk IL are also shown for comparison. Panel (a) indicates the results at 313 K and the legends are as follows: red line for the confined IL using the atomistic silica potential model; blue line for the confined IL using the smooth silica potential model; and black line for the bulk IL. Panel (b) is for 373 K and the legends are the same as those in Panel (a).